Supporting Information

Isolation of Mo(V)-dithiolene-radical: An Elusive Intermediate Species Relevant to Catalytic Cycle of Molybdenum Cofactor

Sujit Das,[a] Harsha S. Karnamkkott,[a] Ashitha Kolothumthodi,[a] Jasmin Behera,[a] Soumen Ghosh,[a] and Kartik Chandra Mondal [a,] *

Department of Chemistry, Indian Institute of Technology Madras, Chennai 600036, India. **E-mail:** csdkartik@iitm.ac.in

Content:

1. **General Synthesis and Characterisation**
2. **Synthesis**
3. **UV-Vis-NIR Measurements**
4. **IR Spectra**
5. **EPR Measurements**
6. **CV Measurements**
7. **Single-Crystal X-ray Diffraction**
8. **Thermogravimetric Analysis**
9. **XPS Measurements**
10. **Computational Methods**
11. **NMR Spectra**
12. **Optimised Coordinates**
13. **References**

1. General Synthesis and Characterisation

The synthesis of air-sensitive compounds was conducted under a purified argon atmosphere utilising Schlenk techniques and an inert-atmosphere drybox (M-Braun LabMaster SP). Chemicals were obtained from Aldrich. All the organic solvents (THF, *n*-hexane, toluene, C_6D_6) were soaked with 3 Å molecular sieves to remove water, followed by distillation with Na metal and NaK alloy three times under the flow of high-purity argon gas. All manipulations were performed inside the dry box, which was run on argon gas at a H_2O/O_2 level of 10 ppm.

The dithiolene radical anion $LS^{\bullet-}$ was prepared by following the previously reported synthetic method.[S1] The selenium analogue of the dithiolene radical anion $LSe^{\bullet-}$ was synthesised by our research group and reported here.[S2] An X-ray single crystal mounted was performed using paratone oil under a flow of argon gas, and data was collected in a Bruker D8 VENTURE model (machine) at 100 and 150 K. Data was refined using the Apex-4 package.

Complexes **1** and **2** are isostructural. The chemical formula is very similar, $C_{54}H_{68}MoN_4OS_6$ (**1**) and $C_{54}H_{68}MoN_4OS_4Se_2$ (**2**). The single crystals were separated by filtration and grinded well before applying vacuum for 2 h at room temperature to remove any volatile solvent. These samples were used for all characterizations.

2. Synthesis

In a 100 mL Schlenk flask, 72 mg (0.2 mmol) of $MoCl_2O_2(DMSO)$ was dissolved in 18 mL of THF and stirred to obtain a homogeneous solution. Then, 253 mg (0.4 mmol) of the ligand $[Mo(V)(O)(LS^{2-})(LS^{\bullet-})]$ (**1**) was added. The colour of the solution did not change significantly at first. To ensure complete reaction, the mixture was stirred for 24 h. During this time, the colour gradually changed from purple to greenish-purple and finally to greenish-brown.

The mixture was then filtered to remove any unreacted material. The filtrate was concentrated and left for crystallisation. Crystals formed the next day, giving a comparatively higher yield (45%). This method is slightly better than the main method, as it avoids low-temperature conditions, the use of KCp*, and hexane, and reduces overall reaction time.

Elemental analysis C, H, N for $C_{54}H_{68}MoN_4OS_6$ (**1**):

Calculated from formula (%): C 60.02, H 6.36, N 5.20.

(Observed, %): C, 60.11; H, 6.29; N, 5.27

IR (KBr; cm^{-1}): 3069, 2962, 2860, 2355, 1630, 1593, 1465, 1403, 1387, 1361, 1361, 1317, 1282, 1196, 1104, 1020, 953, 802, and 421. KBr powders were dehydrated at 250 °C under high vacuum before sample preparation. A KBr pellet was prepared inside the glove box at rt.

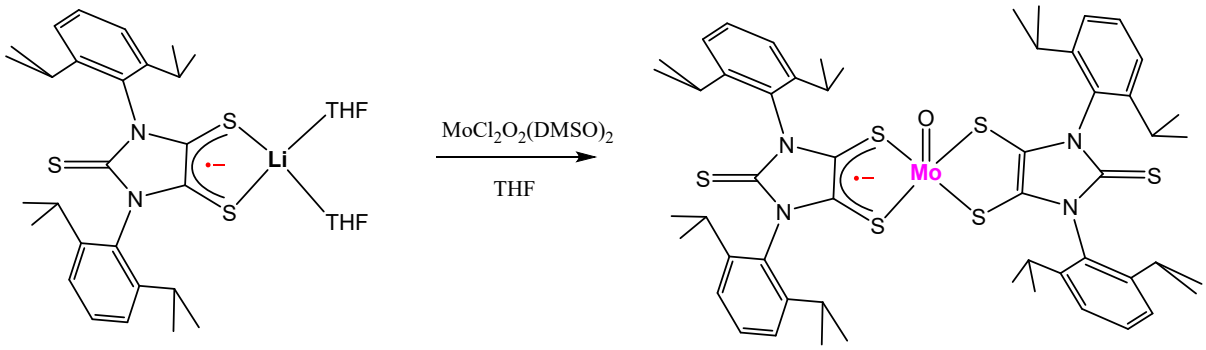

Scheme S1. Synthesis of complex [Mo(V)(O)(LS^{2-})($LS^{\bullet-}$)] (**1**).

Alternative synthesis of complex 1:

Synthesis of [Mo(V)(O)(LS^{2-})($LS^{\bullet-}$)] (**1**): In a 100 mL Schlenk flask, 126 mg (0.2 mmol) of ligand (**$LS^{\bullet-}$**) was dissolved in 20 mL of THF and cooled to –40 °C. $MoOCl_3(THF)_2$ (146 mg, 0.4 mmol) and KCp* (70 mg, 0.4 mmol) were added simultaneously to the cooled ligand solution. The mixture was gradually warmed to room temperature, resulting in a colour change from purple to greenish-black. The reaction was stirred overnight to ensure completion. The solvent was removed under reduced pressure, and the residue was extracted with 15 mL of hexane, producing a brownish-purple solution. The volume was reduced, and the solution was left to crystallise at room temperature, affording dark brown needle-shaped crystals of complex **1** in 38% yield. Pure single crystals were isolated (after removal of mother liquor using a syringe; washed with cold *n*-hexane), which were ground to form powders required for all other characterisations (EPR, UV and CV).

UV-VIS-NIR bands (THF): 416, 566, 657, and 901 nm.

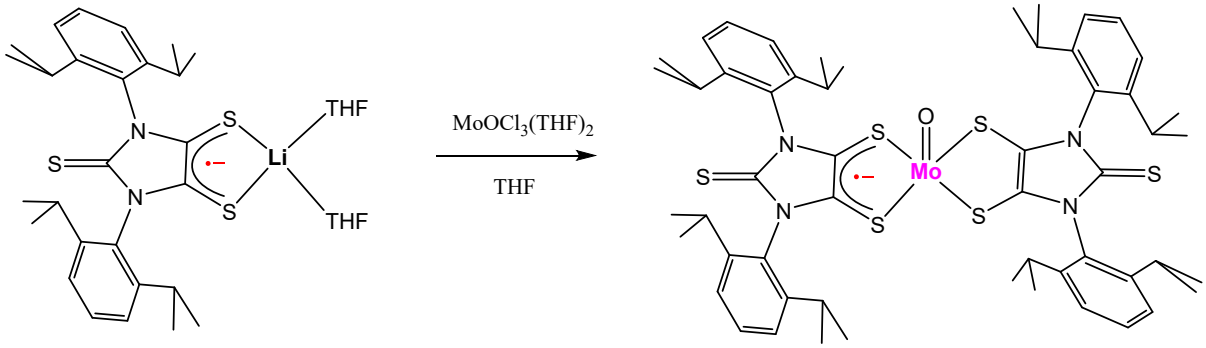

Scheme S2. Synthesis of complex [Mo(V)(O)(LS^{2-})($LS^{\bullet-}$)] (**1**).

Synthesis of complex [Mo(V)(O)(LSe^{2-})($LSe^{\bullet-}$)] (**2**):

The synthesis of complex **2** was carried out by dissolving 270 mg (0.4 mmol) of the ligand **($LSe^{\bullet-}$)** in 20 mL of THF within a 100 mL Schlenk flask under an inert atmosphere. To this solution, 73 mg (0.2 mmol) of $MoOCl_3(THF)_2$ was added, resulting in an immediate colour change from blue to purple, indicative of complex formation. The reaction mixture was stirred at room temperature for 4 h to ensure complete coordination. Subsequent removal of the solvent under reduced pressure afforded a residue, which was extracted with 15 mL of hexane to yield a brownish-purple solution. Concentration of this solution followed by crystallisation at ambient temperature yielded dark brown needle-shaped crystals of complex **2** in 30% isolated yield. Pure colored single crystals were isolated (after removal of mother liquor using a syringe; washed with cold *n*-hexane), which were ground to form powders required for all other characterisations (EPR, UV, and CV).

Elemental analysis C, H, N for $C_{54}H_{68}MoN_4OS_4Se_2$ (**2**):

Calculated from formula (%): C 55.37, H 5.85, N 4.78.

(Observed, %): C, 55.41; H, 5.78; N, 4.85

IR (KBr; cm^{-1}): 2963, 2376, 2347, 1633, 1584, 1424, 1384, 1259, 1107, 1020, 801, 461 and 419. KBr powders have been dehydrated at 250°C under high vacuum before sample preparation. A KBr pellet was prepared inside the glove box at rt.

UV-VIS-NIR bands (THF): 453, 682, and 980 nm.

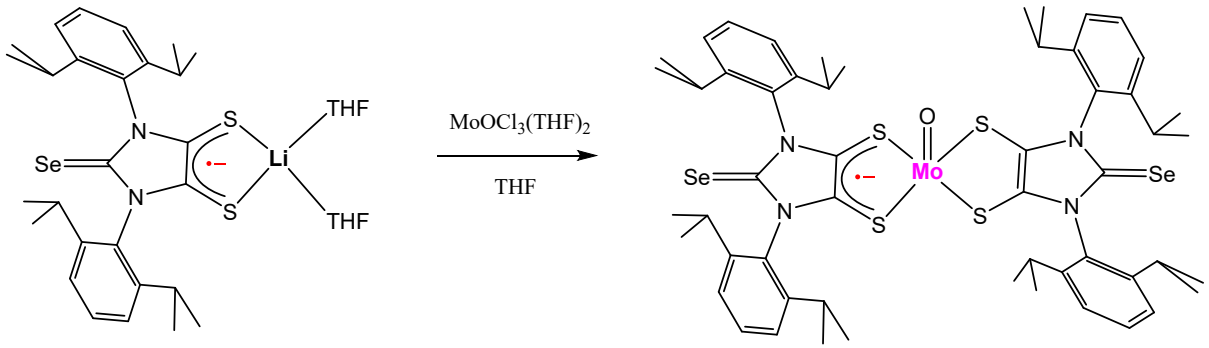

Scheme S3. Synthesis of complex [Mo(V)(O)(LSe^{2-})($LSe^{\bullet-}$)] (**2**).

3. UV-Vis-NIR Measurements

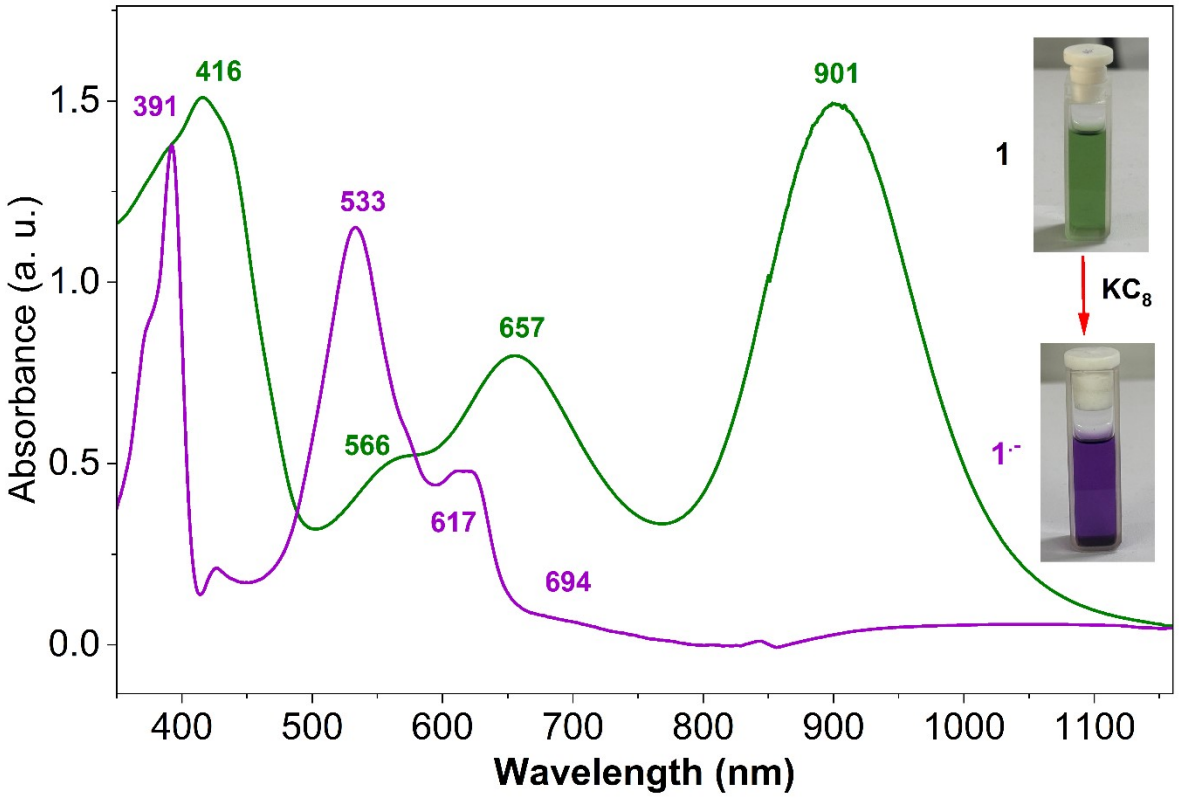

Figure S1. UV-Vis-NIR absorption spectra of complex **1** and its one-electron-reduced form **1**$^{\bullet-}$ recorded in THF solution. The spectrum shown in green corresponds to complex **1**, while the purple trace represents **1**$^{\bullet-}$, generated *in situ* by the addition of one equivalent of KC_8 relative to **1**. The reduction is accompanied by a distinct colour change from green to purple, consistent with the formation of the reduced species.

Molar extinction coefficient of [Mo(V)(O)(LS^{2-})(LS$^{\bullet-}$)] (**1**):

901 nm: 2.48×10^3 L mol^{-1} cm^{-1}

657 nm: 1.4×10^3 L mol^{-1} cm^{-1}

566 nm: 2.87×10^3 L mol^{-1} cm^{-1}

416 nm: 2.52×10^3 L mol^{-1} cm^{-1}

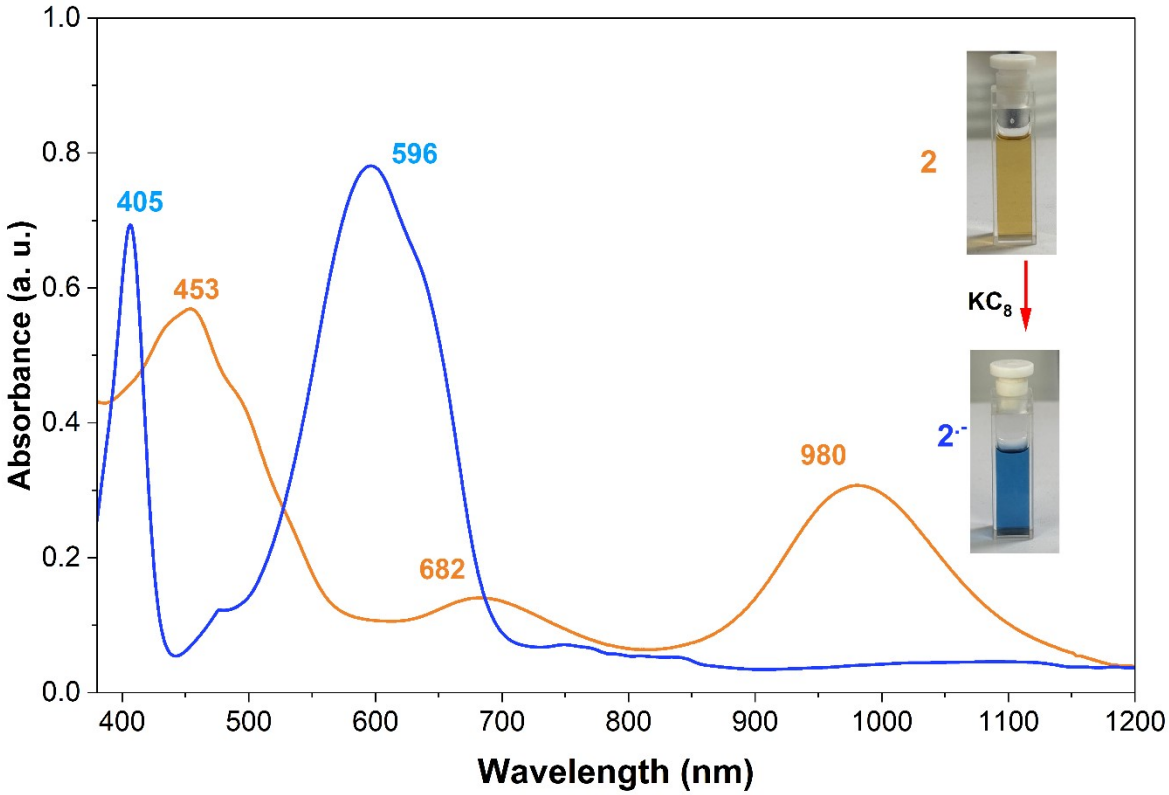

Figure S2. UV-Vis-NIR absorption spectra of complex **2** and its one-electron-reduced form **2**$^{\bullet-}$ recorded in THF solution. The spectrum shown in olive brown corresponds to complex **2**, while the blue trace represents **2**$^{\bullet-}$, generated *in situ* by the addition of one equivalent of KC_8 relative to **2**. The reduction is accompanied by a distinct colour change from olive brown to blue, consistent with the formation of the reduced species.

Molar extinction coefficient of [Mo(V)(O)(LSe^{2-})(LSe$^{\bullet-}$)] (**2**):

980 nm: 1.2×10^{3} L mol^{-1} cm^{-1}

682 nm: 5.0×10^{2} L mol^{-1} cm^{-1}

453 nm: 2.0×10^{3} L mol^{-1} cm^{-1}

4. IR Spectra

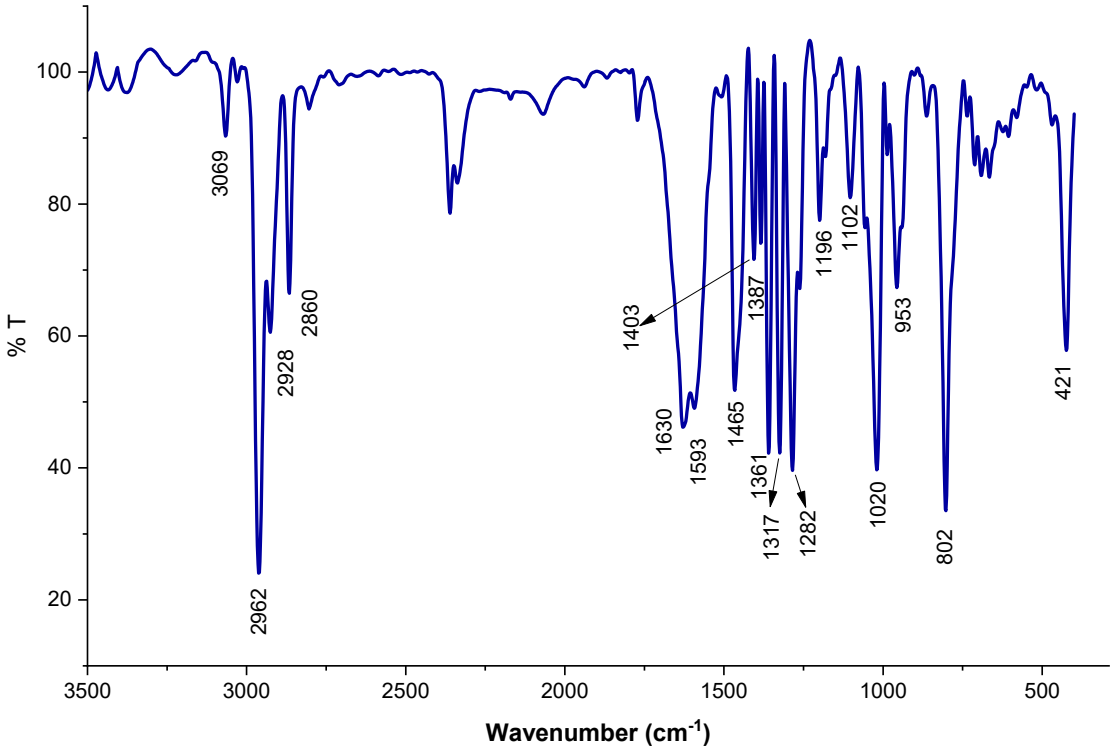

Figure S3. FT-IR spectrum of [Mo(V)(O)(LS^{2-})($LS^{\bullet-}$)] (**1**) with dry KBr.

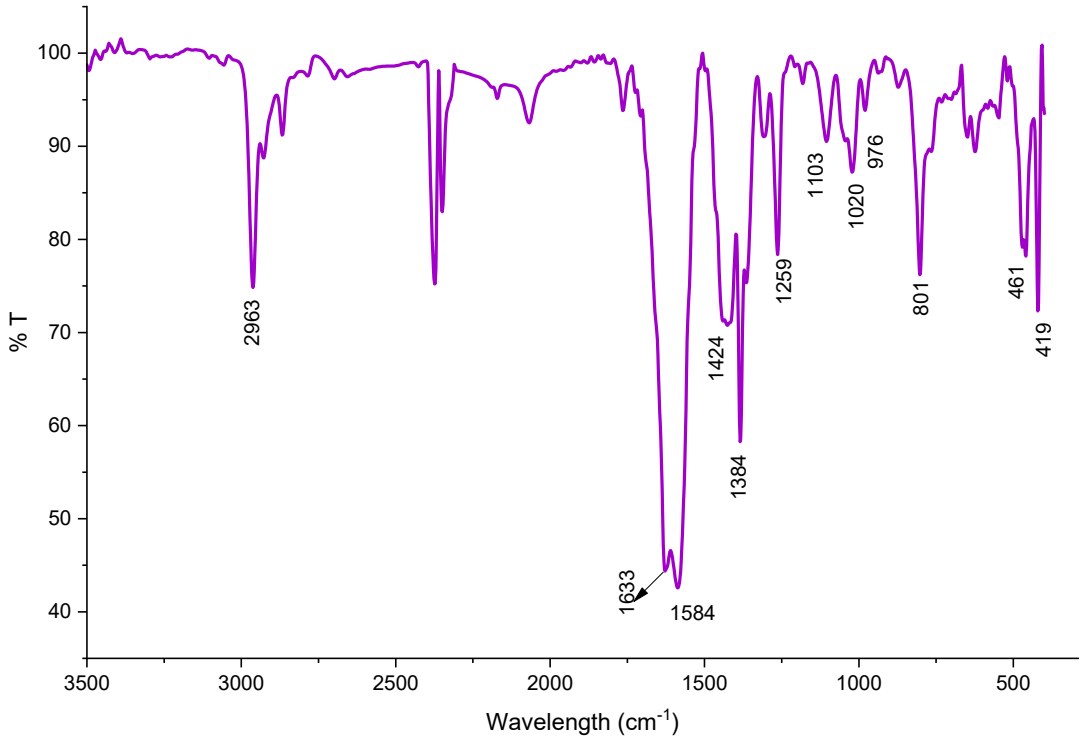

Figure S4. FT-IR spectrum of [Mo(V)(O)(LSe^{2-})(LSe$^{\bullet-}$)] (**2**) with dry KBr.

5. EPR Measurements

The anionic complex **1**$^{-}$ was generated in solution by reacting [Mo(V)(O)(LS^{2-})(LS$^{\bullet-}$)] (**1**) with one equivalent of KC_8 in THF solution. Similarly, the anionic complex **2**$^{-}$ was generated in solution by reacting [Mo(V)(O)(LSe^{2-})(LSe$^{\bullet-}$)] (**2**) with one equivalent of KC_8 in THF solution. The EPR spectrum was simulated with EasySpin package.[S3] The spin Hamiltonian was followed from the textbook by P. Bertrand.[S4] The EPR spectra are in accordance with the Mo-dithiolene based complexes of Hille and Kirk et al.[S5] The hyperfine coupling constants are in good agreement with those of previously reported Mo(V)-dithiolene complexes.[S6] The rhombic nature of the EPR spectrum was explained by Westmoreland et al.[S7]

X-band EPR measurement of complex **2**$^{-}$ (Figure S8) at liquid nitrogen temperature in THF solution exhibits rhombic signal which shows three distinct peaks with g_{isor} = 1.95849 along with hyperfine coupling due to spin active isotopes (^{95,97}Mo) of Molybdenum having hyperfine splitting constants, $A_x(^{95,97}Mo)$ = 107.62, $A_y(^{95,97}Mo)$ = 0, $A_z(^{95,97}Mo)$ = 89.53 MHz. This spectrum is consistent with the spectrum of Mo(V)-dithiolene complexes[S5-S6] having the

hyperfine coupling constants 87-111 MHz which were previously reported for molybdenum complexes.[S5] The EPR spectrum is in agreement with the coordination geometry of anionic complexes (**1**$^{-}$ and **2**$^{-}$).

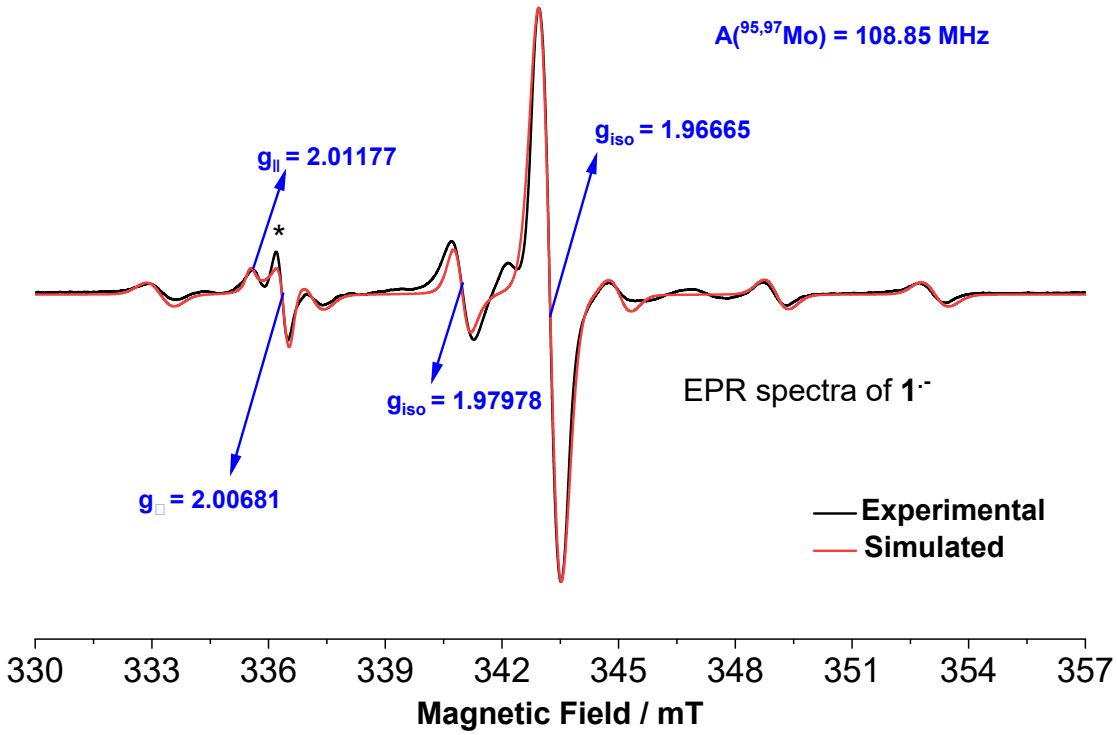

Figure S5. X-band EPR spectrum (black) of complex [Mo(V)(O)(LS^{2-})$_2$] (**1**$^{-}$) at room temperature in THF solvent. Red and black lines represent the simulated and experimental spectra of anionic complex **1**$^{-}$ and the simulation is done using the EasySpin program.[S3] [*Due to Mo unpaired electron*: $\mathbf{g_{iso}}$ = 1.96665, LWPP (Gaussian broadening) = 0.55 mT, LWPP (Lorentzian broadening) = 0.076 mT, **A**(^{95,97}Mo) = 108.85 MHz. **[**X-band experimental frequency = 9.4478 GHz**]**

Other conformations of **1**$^{-}$ or radical impurity: at $\mathbf{g_{\perp}}$ = 2.00681, $\mathbf{g_{\parallel}}$ = 2.01177, LWPP (Gaussian broadening) = 0.14 mT, LWPP (Lorentzian broadening) = 0.13 mT, and at **g** = 1.97978, LWPP (Gaussian broadening) = 0.39 mT, LWPP (Lorentzian broadening) = 0.011 mT, X-band experimental frequency = 9.4478 GHz].

$$g_{iso} = \sqrt{\frac{2g_{\perp}^{2} + g_{\parallel}^{2}}{3}} = \sqrt{\frac{2 \times 2.00681^{2} + 2.01177^{2}}{3}} = 2.00846$$

Hamiltonian:

$$\hat{H} = g\beta S \cdot B$$

$$\hat{H} = g\beta S \cdot B \; + \; A_{Mo} S \cdot I_{Mo}$$

$$\hat{H} = \beta[g_{\perp}(\hat{S}_x B_x + \hat{S}_y B_y) + g_{\parallel} \hat{S}_z B_z]$$

These Hamiltonian models used for the simulation shown in Figure 5 and is consistent with Equations 3.12, and 3.22 of reference S4. The term $\mu_B gS \cdot B$ represents the electron Zeeman interaction, which dominates the spectral features in this system. $A_{Mo} S \cdot I_{Mo}$ represents the hyperfine coupling between the unpaired electron and the spin-active isotopes of molybdenum. The use of two distinct g-values, which represent the signal at around 336 mT reflects the axial anisotropy, implying that the electronic environment is symmetric around a unique principal axis (z-axis), while the x and y directions are equivalent ($g_x = g_y = g_{\perp}$). This form of the Hamiltonian is consistent with the axial g-tensor approximation commonly employed for transition metal complexes and radical systems, and is in agreement with section 6.3 of reference S4.

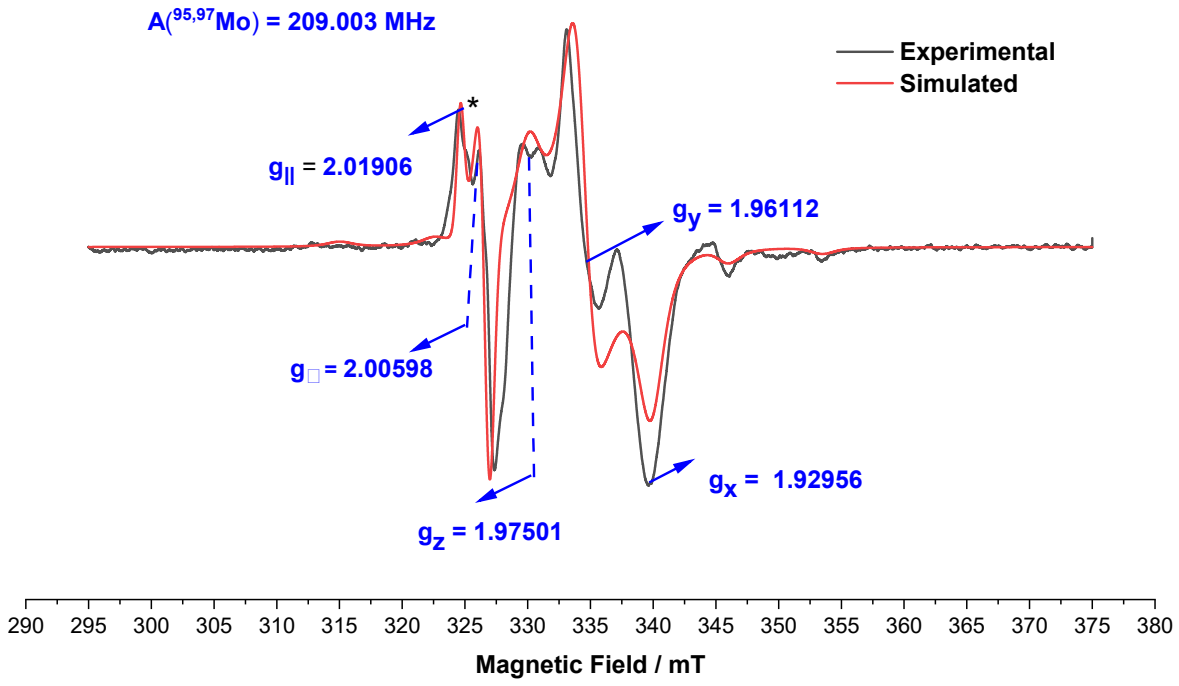

Figure S6: X-band EPR spectrum (black) of complex [Mo(V)(O)(LS^{2-})$_2$] (**1**$^{-}$) at liquid nitrogen temperature in THF solvent. Red and black lines represent the simulated and experimental spectra of anionic complex **1**$^{-}$ and the simulation is done using the EasySpin program. $\mathbf{g_x}$ = 1.92956, $\mathbf{g_y}$ = 1.96112, $\mathbf{g_z}$ = 1.97501, $\mathbf{\Delta g_z}$ (g-strain) =0.001, LWPP (Gaussian broadening) = 1.0017 mT, LWPP (Lorentzian broadening) = 0.981 mT, $\mathbf{A_y}$ (^{95,97}Mo) = 209.003 MHz, $\mathbf{A_z}$(^{1,2}H) = 100.0 MHz**.**

Other possible conformations of **1**$^{-}$: $\mathbf{g_\perp}$ = 2.00598, $\mathbf{g_\parallel}$ = 2.01906, g strain; $\mathbf{\Delta g_\perp}$ = 0.006, $\mathbf{\Delta g_\parallel}$ = 0.004, LWPP (Gaussian broadening) = 0.051 mT, LWPP (Lorentzian broadening) = 0.050 mT, X-band experimental frequency = 9.1744 GHz].

$$g_{iso} = \sqrt{\frac{g_x{}^2 + g_y{}^2 + g_z{}^2}{3}} = \sqrt{\frac{1.92956^2 + 1.96112^2 + 1.97501^2}{3}} = 1.95532$$

$$g_{iso} = \sqrt{\frac{2g_\perp{}^2 + g_\parallel{}^2}{3}} = \sqrt{\frac{2 \times 2.00598^2 + 2.01906^2}{3}} = 2.01034$$

Hamiltonian:

$$\hat{H} = \beta(g_x \hat{S}_x B_x + g_y \hat{S}_y B_y + g_z \hat{S}_z B_z) + \Sigma_k A_k S \cdot I_{k(k=Mo)}$$

$$\hat{H} = \beta[g_\perp (\hat{S}_x B_x + \hat{S}_y B_y) + g_\parallel \hat{S}_z B_z]$$

The Hamiltonian used for the simulation in the figure, follows Equation 3.15 of reference S4, with Equation 7.27 extended to include hyperfine interactions. The presence of three distinct g-values ($g_x \neq g_y \neq g_z$), indicates a fully anisotropic (rhombic) magnetic environment, reflecting a low-symmetry paramagnetic center. The first term represents the electron Zeeman interaction, while the second one accounts for hyperfine coupling between the unpaired electron and molybdenum nuclei, indicating significant spin localization at the metal center, consistent with Mulliken spin densities.

The second Hamiltonian model uses two g-values as described in Section 6.3 of reference S4, representing axial anisotropy, implying equivalent magnetic response in the x and y directions $(g_x = g_y = g_\perp)$ and a different response along the z direction $(g_z = g_\parallel)$.

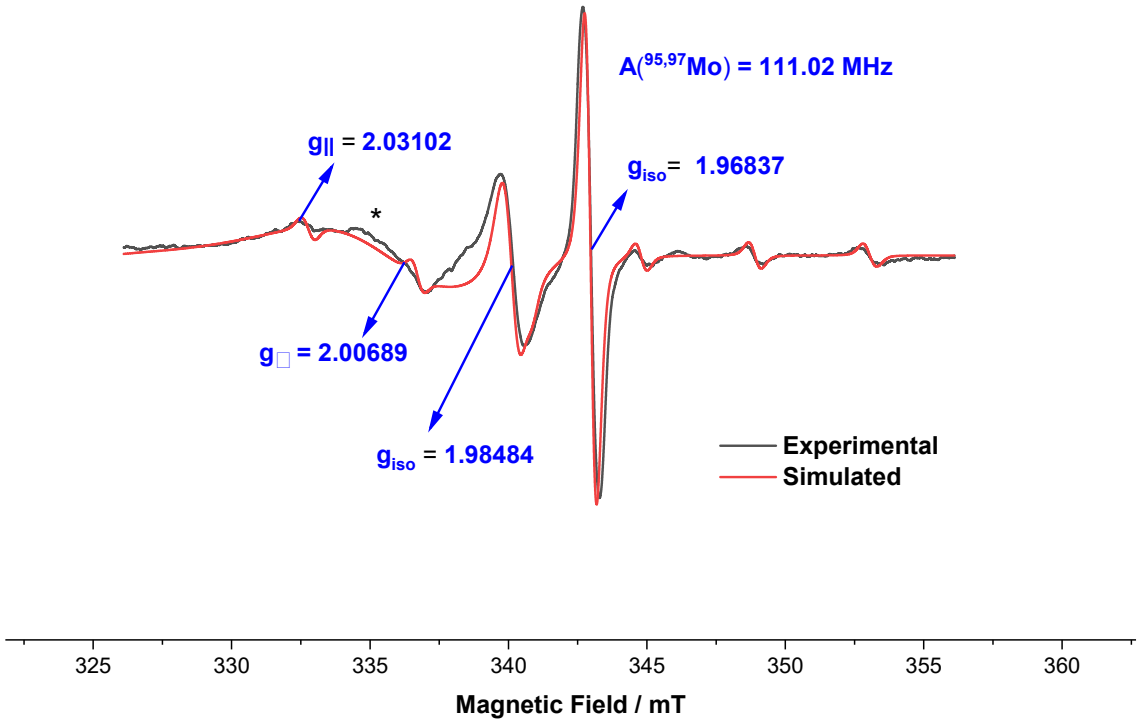

Figure S7. X-band EPR spectrum (black) of complex [Mo(V)(O)(LS^{2-})$_2$] (**2**$^{-}$) at room temperature in THF solvent. Red and black lines represent the simulated and experimental spectra of anionic complex **1**$^{\bullet-}$ and the simulation is done using the EasySpin program.[S3] [*Due to Mo unpaired electron*: $\mathbf{g_{iso}}$ = 1.96837, LWPP (Gaussian broadening) = 0.35 mT, LWPP (Lorentzian broadening) = 0.15 mT, **A**(^{95,97}Mo) = 111.02 MHz. For EPR signal at $\mathbf{g_{iso}}$ = 1.98484: $\mathbf{g_{\perp}}$ = 2.00689, g strain; $\mathbf{g_{\parallel}}$ =2.03102, $\mathbf{\Delta g_{\perp}}$ = 0.03, $\mathbf{\Delta g_{\parallel}}$ = 0.05, LWPP (Gaussian broadening) = 0.03 mT, LWPP (Lorentzian broadening) = 0.05 mT, $\mathbf{g_{iso}}$ = 1.98484, LWPP (Gaussian broadening) = 0.46 mT, LWPP (Lorentzian broadening) = 0.40 mT, X-band experimental frequency = 9.4487 GHz].

$$g_{iso} = \sqrt{\frac{2g_{\perp}^{2} + g_{\parallel}^{2}}{3}} = \sqrt{\frac{2 \times 2.00689^{2} + 2.03102^{2}}{3}} = 2.01496$$

Hamiltonian:

$$\hat{H} = g\beta S \cdot B$$

$$\hat{H} = g\beta S \cdot B \; + \; A_{Mo} S \cdot I_{Mo}$$

$$\hat{H} = \; \beta[g_{\perp}(\hat{S}_x B_x + \hat{S}_y B_y) + \; g_{\parallel} \hat{S}_z B_z]$$

The Hamiltonian model used for the simulation in Figure 7 is consistent with Equations 3.12, 3.22, and section 6.3 of reference S4. The term $\mu_B \, gS \cdot B$ corresponds to the electron Zeeman interaction, which is the primary contributor to the observed spectral features. The term $A_{Mo} S \cdot I_{Mo}$ describes the hyperfine interaction between the unpaired electron and the spin-active molybdenum nuclei.

The presence of two distinct g-values around 332 mT, indicates axial anisotropy. This suggests that the electronic environment is symmetric about a single principal axis (z-axis), while the x and y directions remain equivalent $(g_x = g_y = g_{\perp})$.

The observed differences in the EPR spectra of anionic form the complexes **1**$^{-}$ (Figure S5) and **2**$^{-}$ (Figure S6) primarily arise from mostly Mo(V) [^{95,97}Mo, I = 3/2] of [Mo(V)(LE^{2-})$_2$]$^{-}$ centre environment, specifically the substitution of sulfur (S) in complex **1** by selenium (Se) in complex **2** in the C2 position of NHC. The sharp signal in the middle is due spin inactive 76% Mo(V) nucleus of **1**$^{-}$/**2**$^{-}$. Four satellites of ~24% spin active ^{95,97}Mo, (I = 3/2) nucleus. This feature is clearly visible for anionic **1**$^{-}$ while a similar feature is also observed for **2**$^{-}$. The additional feature at $\mathbf{g_{iso}}$ = 1.98484 could be due to the conformational isomer of **2**$^{-}$ which is symmetrical when the distributions of spin densities were concerned. The rhombic nature of the EPR spectrum was explained by Westmoreland et al.[S7s] Two conformation eventually become one when cooled to 77 K as seen in Figure S8.

MtsZ is Mo-containing methionine sulfoxide reductase in Haemophilus influenzae (Hi) which regulates virulence in the human respiratory pathogen. Kappler et al[S7b] have studied coordination sphere flexibility in the protein structure at the MoO site of HiMtsZ. They also have recorded X-band EPR spectra of HiMtsZ during redox titration. One of the EPR spectra closely resemble to those of Figures S6 and S8.[S7b] The Mo(V) related UV-vis band of HiMtsZ shows an absorption band near 670 nm.[S7b]

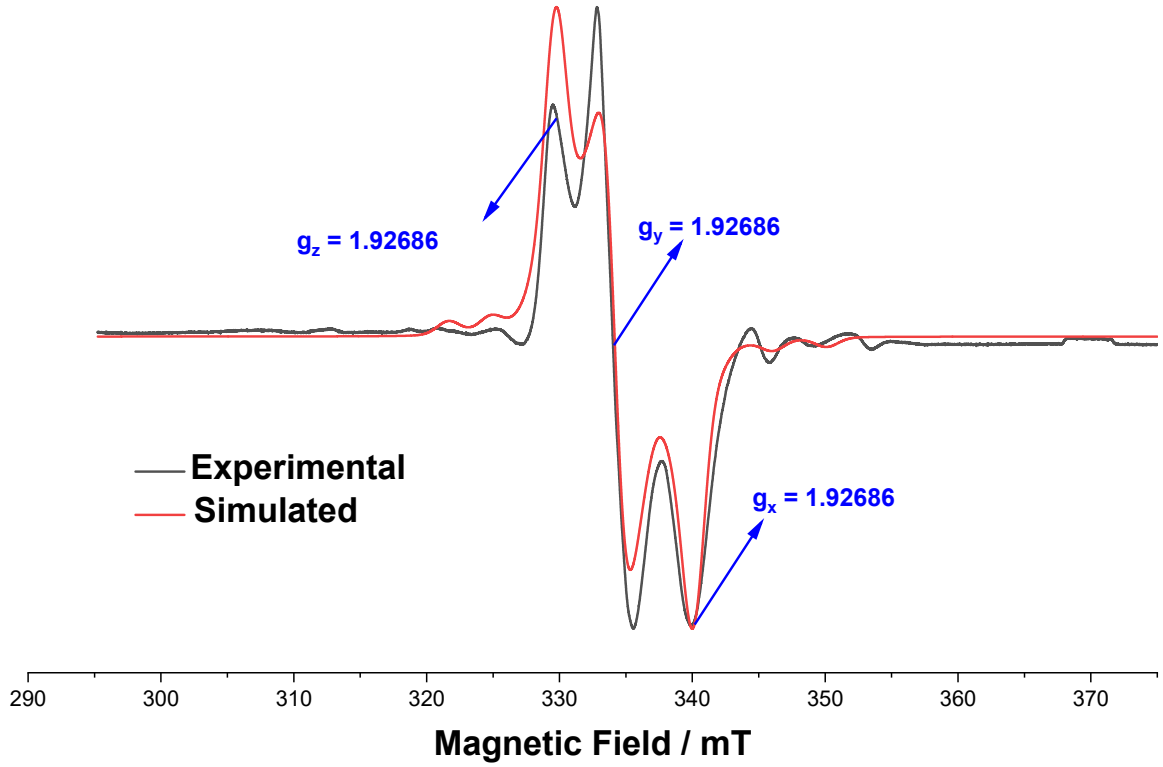

Figure S8. X-band EPR spectrum (black) of anionic complex **2**$^{-}$ at liquid nitrogen temperature in THF solvent. Red and black lines represent the simulated and the experimental spectra of **2**$^{\bullet-}$ and the simulation is done using the EasySpin program.[S3] [$\mathbf{g_x}$ = 1.92686, $\mathbf{g_y}$ = 1.96097, $\mathbf{g_z}$ = 1.98716, LWPP (Gaussian broadening) = 1.53 mT, LWPP (Lorentzian broadening) = 0.25 mT, $\mathbf{A_x}(^{95,97}\text{Mo})$ = 107.62, $\mathbf{A_y}(^{95,97}\text{Mo})$ = 0, $\mathbf{A_z}(^{95,97}\text{Mo})$ = 89.53 MHz, X-band experimental frequency = 9.1718 GHz]. See reference S6 for rhombic EPR spectrum in frozen state.

$$g_{iso} = \sqrt{\frac{{g_x}^2 + {g_y}^2 + {g_z}^2}{3}} = \sqrt{\frac{1.92686^2 + 1.96097^2 + 1.98716^2}{3}} = 1.95849$$

Hamiltonian:

$$\hat{H} = \beta(g_x \hat{S}_x B_x + g_y \hat{S}_y B_y + g_z \hat{S}_z B_z) + \Sigma_k A_k S \cdot I_{k(k=Mo)}$$

This Hamiltonian model was used for the simulation shown in Figure 8 and is consistent with Equation 3.15 of reference S4, and represents an extension of Equation 7.27 to include hyperfine interactions. The use of three distinct g-values reflects a fully anisotropic (rhombic)

magnetic environment ($g_x \neq g_y \neq g_z$), indicating a low-symmetry electronic structure of the paramagnetic centre.

The first term represents the electron Zeeman interaction, while the second term accounts for hyperfine coupling between the unpaired electron and the molybdenum nuclei, indicating significant localisation of spin density at the metal centre, which is in agreement with the Mulliken spin density distributions.

6. CV measurement:

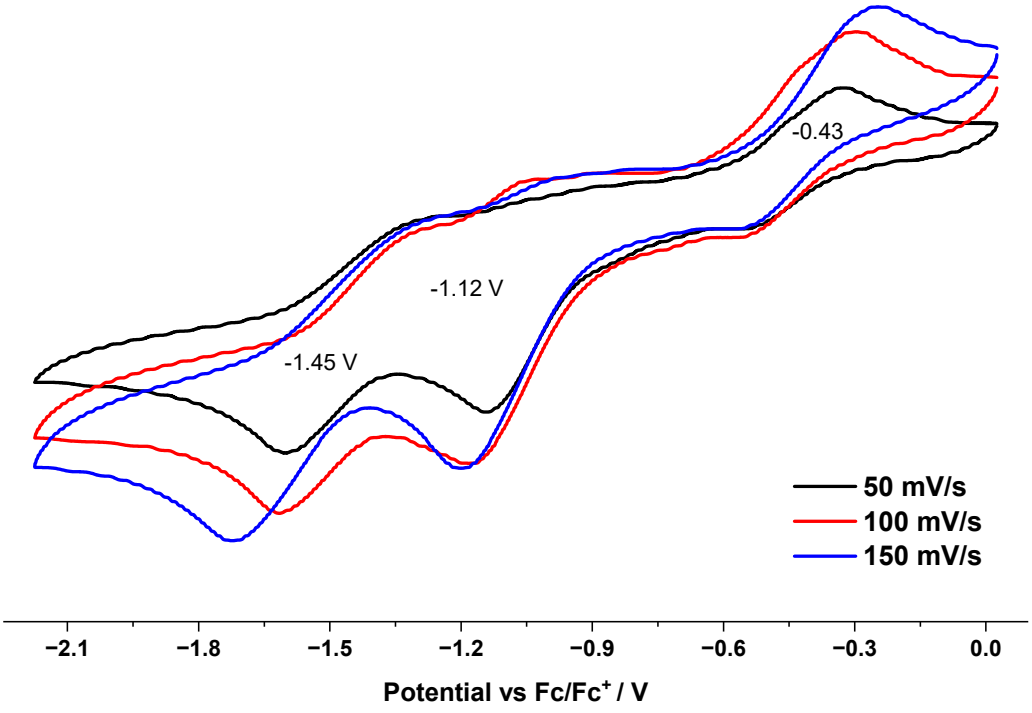

Figure S9. Cyclic voltammogram of complex [Mo(V)(O)(LS^{2-})($LS^{\bullet-}$)] (**1**) in THF solution of 0.1 M [*n*-Bu_4N]PF_6 with RE: Ag, WE: GC, and CE: Pt.

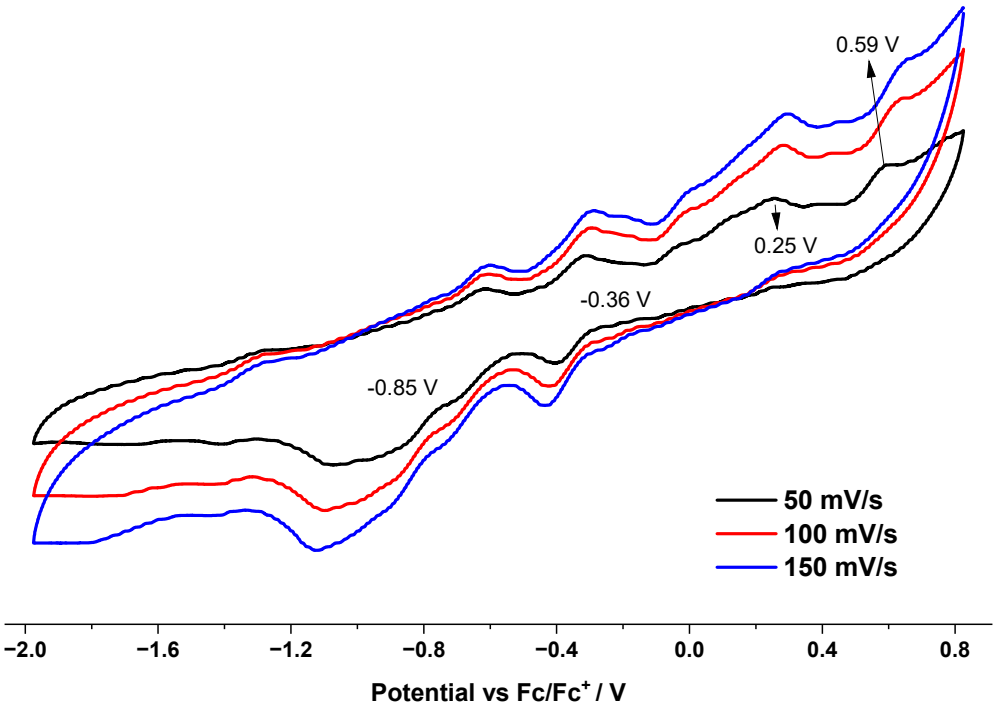

Figure S10. Cyclic voltammogram of complex [Mo(V)(O)(LSe^{2-})($LSe^{\bullet-}$)] (**2**) in THF solution of 0.1 M [*n*-Bu_4N]PF_6 with RE: Ag, WE: GC, and CE: Pt.

Complex **2** exhibits a different cyclic voltametric behaviour due to the distinct nature of the ligand ($LE^{\bullet-}$, E = Se). The free radical ligand ($LSe^{\bullet-}$) shows two quasi-reversible redox couples at +0.14 V ($^{\Delta E_p}$= 0.17 V) and –0.50 V ($^{\Delta E_p}$= 0.16 V), which are assigned to the [$L^0/L^{\bullet-}$] and [$L^{\bullet-}/L^{2-}$] processes, respectively. In contrast, for complex **2**, these ligand-based redox processes are shifted to more negative potentials, appearing at –0.36 V ($^{\Delta E_p}$= 0.20 V) and –0.85 V ($^{\Delta E_p}$= 0.17 V), corresponding to the same [$L^{\circ}/L^{\bullet-}$] and [$L^{\bullet-}/L^{2-}$] couples. Additionally, two redox waves observed at +0.25 V and +0.59 V are attributed to metal-centred processes. However, these processes are completely irreversible, making it difficult to determine the exact number of electrons involved in the metal redox events.

7. Single-Crystal X-ray Diffraction

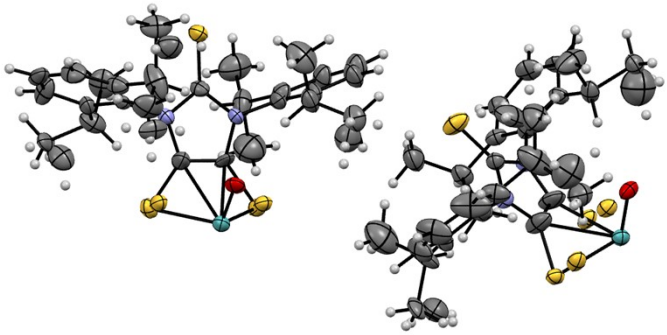

(a)

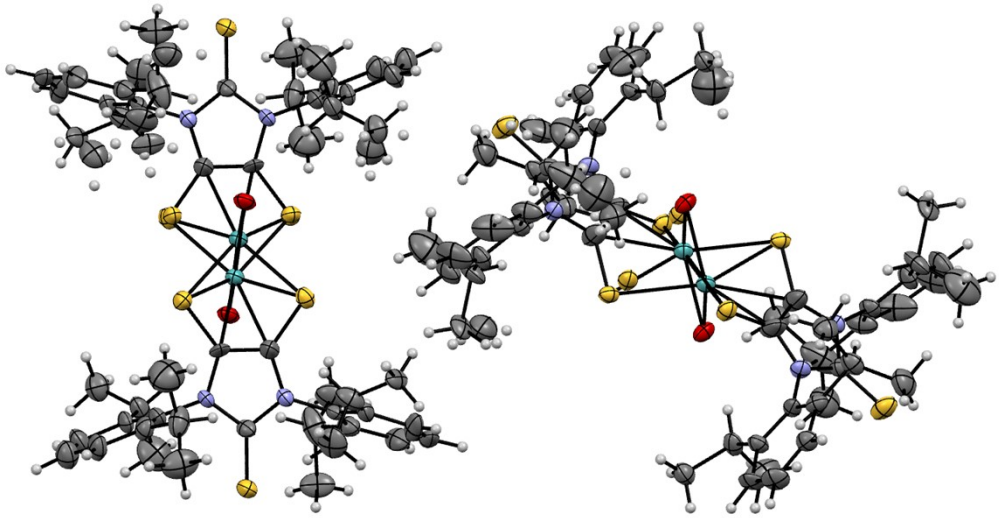

(b)

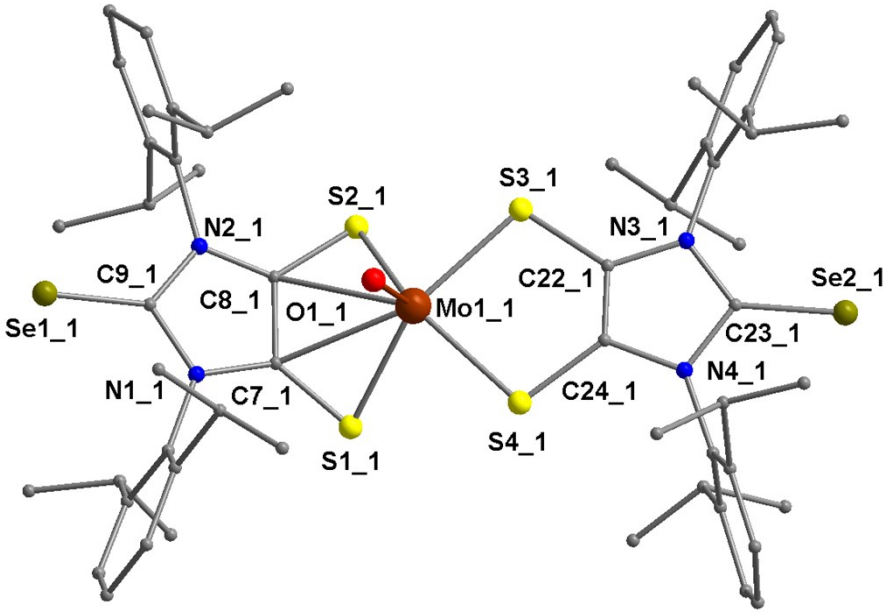

(c)

Figure S11. (a) Two independent half molecules of complex **1** in the asymmetric crystallographic unit (second set of data). (b) Two independent complete molecules of complex **1** (second set of data). (c) Molecular structure of complex [Mo(V)(O)(LSe^{2-})($LSe^{\bullet -}$)] (**2**). All

the H atoms were omitted for clarity. The structure of **2** has been given for bond connectivity only (see crystallographic Table S2). There are two crystallographically independent molecules are present in the asymmetric crystallographic unit. For clarity only one has been shown here. The single crystals were very small. Repeated data collection did not improve the refinement parameters due to poor diffraction. The structure from crystal grown from toluene was shown here.

Table S1. Crystallographic details of complex [Mo(V)(O)(LS^{2-})($LS^{\bullet-}$)] (**1**).

Complex	**1**	**1**
CCDC Deposit	**2530326**	
Set of data	First set of data	Second set of data
Reaction	THF	*n*-hexane
Crystallization	*n*-hexane	*n*-hexane
Empirical formula	$C_{108}H_{136}Mo_2N_8O_2S_{12}$	$C_{108}H_{136}Mo_2N_8O_2S_{12}$
Formula weight	2154.84	2154.84
Temperature (K)	100 (2)	120 (2)
Wavelength (Å)	0.71073	0.71073
Crystal system	Triclinic	Triclinic
Space group	*P*-1	*P*-1
Unit cell dimensions	*a* = 15.8373(12) Å *b* = 17.6411(14) Å *c* = 23.5371(19) Å *α* = 90.104(3)° *β* = 103.590(2)° *γ* = 106.628(3)°	*a* = 8.8531(11) Å *b* = 15.807(2) Å *c* = 23.577(3) Å *α* = 76.333(5)° *β* = 89.888(5)° *γ* = 74.215(5)°
Volume ($Å^3$)	6107.7(8)	3078.2(7)
Z	2	1
Density (Mg/m^3)	1.172	1.162
Absorption coefficient (mm^{-1})	0.456	0.453
F (000)	2264	1132
Crystal size (mm^3)	0.132 × 0.143 × 0.174	0.017 × 0.038 × 0.169
Theta range for data collection (°)	2.90 to 50.05	4.79 to 50.05
Index ranges	−18 ≤ h ≤ 18 −20 ≤ k ≤ 20 −28 ≤ l ≤ 28	−10 ≤ h ≤ 10 −18 ≤ k ≤ 18 −28 ≤ l ≤ 27
R (int)	0.093	0.1688
Reflections collected	250078	79584
Independent reflections	21530	10657
Completeness to theta = 25.027°	100.0 %	98.2
Max. and min. transmission	0.942 and 0.925	0.7472 and 0.6782
Number of Restraints	200	103
Number of Parameters	1394	757
Refinement method	Full-matrix least-squares on F^2	Full-matrix least-squares on

		F^2
Final R indices [I>2sigma(I)]	R_1 = 0.0669 wR_2 = 0.1475	R_1 = 0.1378 wR_2 = 0.4128
R indices (all data)	R_1 = 0.0854 wR_2 = 0.1578	R_1 = 0.1788 wR_2 = 0.4337
GooF	1.098	1.595
Largest diff. peak and hole [e·Å^{-3}]	0.87 and -0.69	1.45 and -0.69

The X-ray single crystal data was collected two times from two different batches of reaction flasks. The unit cell parameters of complex **1** are completely different from each other (Table S1). The length of the a-axis of is half for the second batch of crystal. While the first set of data had shown the possibility of the presence of the higher-symmetric monoclinic crystal system, but eventually structure solution was only possible triclinic *P*-1 space group. The data of second batch exclusively showed triclinic *P*-1 space group. The first set of data of complex **1** showed better diffraction when they were compared with those of second set of data, [total reflections, 250,078 vs 79,584]. Also, it is clearly visible that the *R*(int) value of the first set of data (0.093) is much lower compared to the second set of data (0.1688). Similarly, the R_1 value of first set of data of complex **1** (0.0669) is significantly lower than that of second set of data (0.1378). In spite of all these striking differences between the two sets of data, both of them contained the same structure, and solved in the same space group *P*-1. Strikingly, second set of data complex **1** contained no alert related to symmetry or space group, which was present in the first set of data.

C-C bond lengths 1.411(6)/1.350(6) Å for first sent of data [stronger diffraction data set].

C-C bond lengths 1.375(15)/1.368(16) Å for second sent of data [relatively weaker diffraction].

Two MoO units in one molecular complex **1** are present. This MoO unit is always incline/tilted towards C_2S_4 unit in both the set of data as theoretically predicted (see computational part).

Table S2. Crystallographic details of complex [Mo(V)(O)(LSe^{2-})($LSe^{\bullet-}$)]·toluene (**2**·toluene).

Empirical formula	$C_{122}H_{150}Mo_2N_8O_2S_8Se_4$
Formula weight	2524.69
Temperature (K)	130(2)
Wavelength (Å)	0.71073
Crystal system	Triclinic
Space group	*P*-1
Unit cell dimensions	*a* = 16.2514(6) Å *b* = 18.1829(6) Å *c* = 26.0279(9) Å *α* = 69.5640(10)° *β* = 82.7970(10)° *γ* = 68.6760(10)°
Volume ($Å^3$)	6713.7(4)
Z	2
Density (Mg/m^3)	1.249
Absorption coefficient (mm^{-1})	1.442
F (000)	2604
Crystal size (mm^3)	0.077 × 0.114 × 0.163
Theta range for data collection (°)	3.82 to 61.77
Index ranges	−22 ≤ h ≤ 22 −21 ≤ k ≤ 25 −36 ≤ l ≤ 35
R (int)	0.0722
Reflections collected	140610
Independent reflections	36327
Completeness to theta = 25.242°	98.4%
Max. and min. transmission	0.7461 and 0.6534
Number of Restraints	0
Number of Parameters	626
Refinement method	Full-matrix least-squares on F^2
Final *R* indices [*I*>2sigma(*I*)]	R_1 = 0.3240 wR_2 = 0.6890
R indices (all data)	R_1 = 0.3667 wR_2 = 0.7118
GooF	3.111
Largest diff. peak and hole [$e·Å^{-3}$]	21.77 and −4.89

Table S3. Selected bond lengths [Å] for the complex [Mo(V)(O)(LS^{2-})($LS^{\bullet-}$)] (**1**).

Mo1–O1	1.682(4)
Mo1–S9	2.375(2)
Mo1–S1	2.379(2)
Mo1–S10	2.4044(17)
Mo1–S12	2.4103(17)
Mo3–O3	1.645(12)
Mo3–S4A	2.363(6)
Mo3–S6A	2.384(5)
Mo3–S5A	2.393(5)
Mo3–S3A	2.406(5)
Mo4–O4	1.679(3)
Mo4–S3	2.3760(17)
Mo4–S5	2.3868(17)
Mo4–S4	2.4026(15)
Mo4–S6	2.4057(14)
Mo5–O2	1.659(9)
Mo5–S11	2.367(4)
Mo5–S12'	2.372(4)
Mo5–S9'	2.407(3)
Mo5–S1A	2.412(3)
C10–C11	1.411(6)
C22–C23	1.350(6)
C62–C63	1.401(6)
C74–C81	1.356(6)

Table S4. Selected bond angles [°] for the complex [Mo(V)(O)(LS^{2-})($LS^{\bullet-}$)] (**1**).

O1–Mo1–S9	110.66(15)
O1–Mo1–S1	110.90(16)
S9–Mo1–S1	92.49(7)
O1–Mo1–S10	105.80(16)

S9–Mo1–S10	143.22(7)
S1–Mo1–S10	78.74(6)
O1–Mo1–S12	107.40(16)
S9–Mo1–S12	78.78(6)
S1–Mo1–S12	141.32(8)
S10–Mo1–S12	86.08(5)
O3–Mo3–S4A	110.5(4)
O3–Mo3–S6A	109.9(4)
S4A–Mo3–S6A	91.9(2)
O3–Mo3–S5A	106.0(5)
S4A–Mo3–S5A	143.2(2)
S6A–Mo3–S5A	79.07(18)
O3–Mo3–S3A	107.6(4)
S4A–Mo3–S3A	79.5(2)
S6A–Mo3–S3A	142.2(2)
S5A–Mo3–S3A	86.10(16)
O4–Mo4–S3	110.80(13)
O4–Mo4–S5	110.74(13)
S3–Mo4–S5	91.85(6)
O4–Mo4–S4	106.45(13)
S3–Mo4–S4	78.62(5)
S5–Mo4–S4	142.58(6)
O4–Mo4–S6	106.55(13)
S3–Mo4–S6	142.26(6)
S5–Mo4–S6	79.75(5)
S4–Mo4–S6	86.03(5)
O2–Mo5–S11	110.4(3)
O2–Mo5–S12'	110.9(3)
S11–Mo5–S12'	92.80(13)
O2–Mo5–S9'	106.0(3)
S11–Mo5–S9'	143.17(15)
S12'–Mo5–S9'	78.90(12)

O2–Mo5–S1A	106.5(3)
S11–Mo5–S1A	79.33(14)
S12'–Mo5–S1A	142.11(17)
S9'–Mo5–S1A	85.56(11)

8. Thermogravimetric Analysis

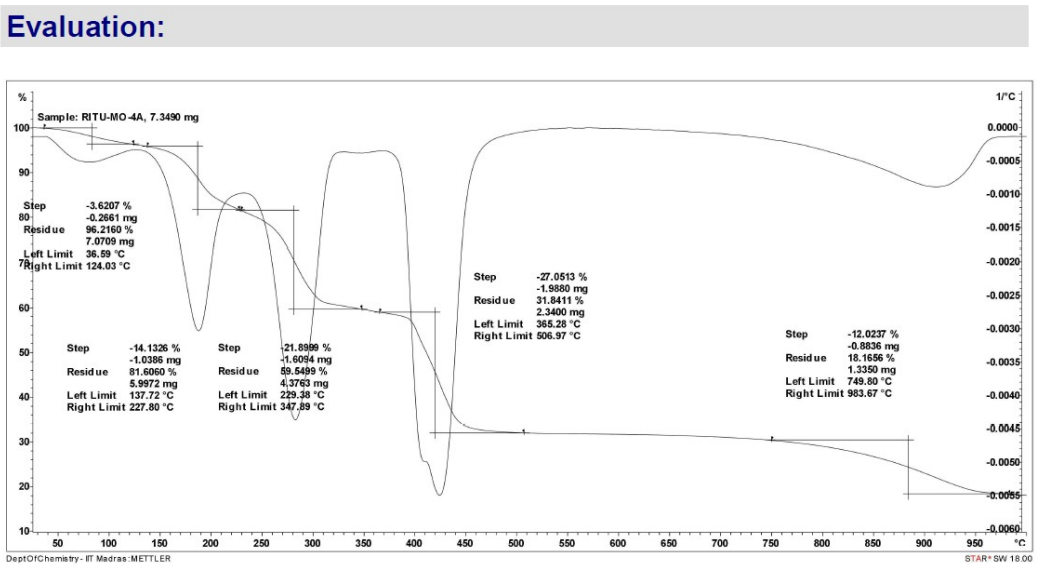

Figure S12. TGA of complex [Mo(V)(O)(LS^{2-})($LS^{\bullet-}$)] (**1**) in open air over 90 min, scanning the temperature from 30 °C to 1000 °C. The initial weight loss is due to possible *n*-hexane in the crystals. The loss of volatile near 60 °C from the powdered samples.

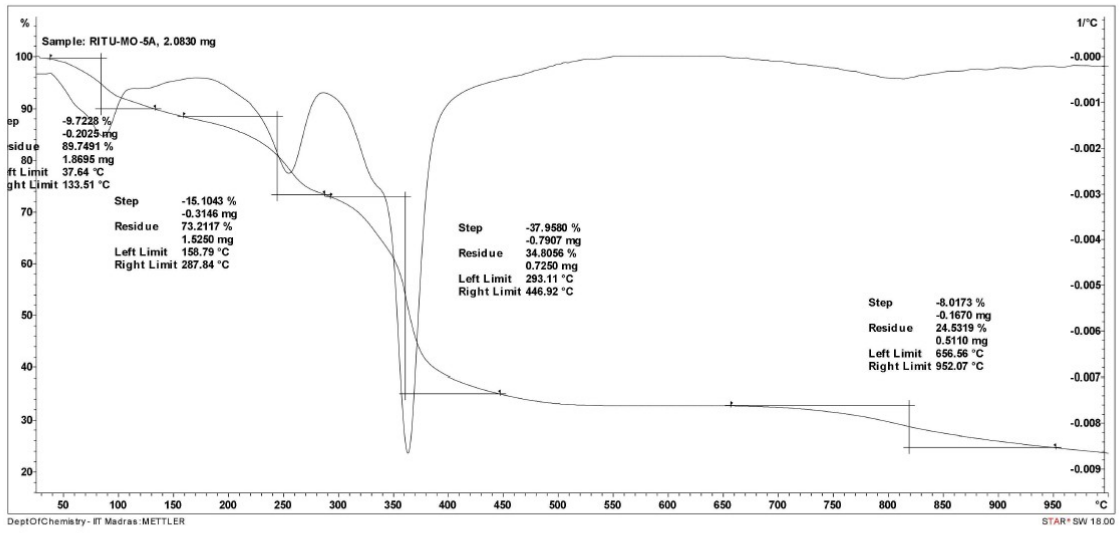

Figure S37. TGA of complex [Mo(V)(O)(LSe^{2-})($LSe^{\bullet-}$)] (**2**) in open air over 90 min, scanning the temperature from 30 °C to 1000 °C. The initial weight loss is due to possible *n*-hexane in the crystals.

9. XPS Measurements

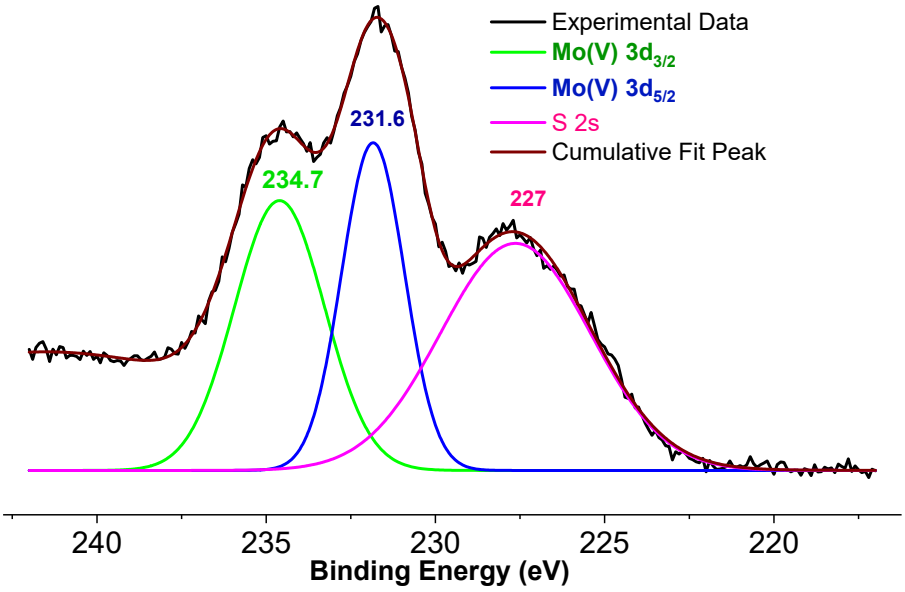

Figure S14. XPS plots of Mo and S of complex [Mo(V)(O)(LS^{2-})($LS^{\bullet-}$)] (**1**).

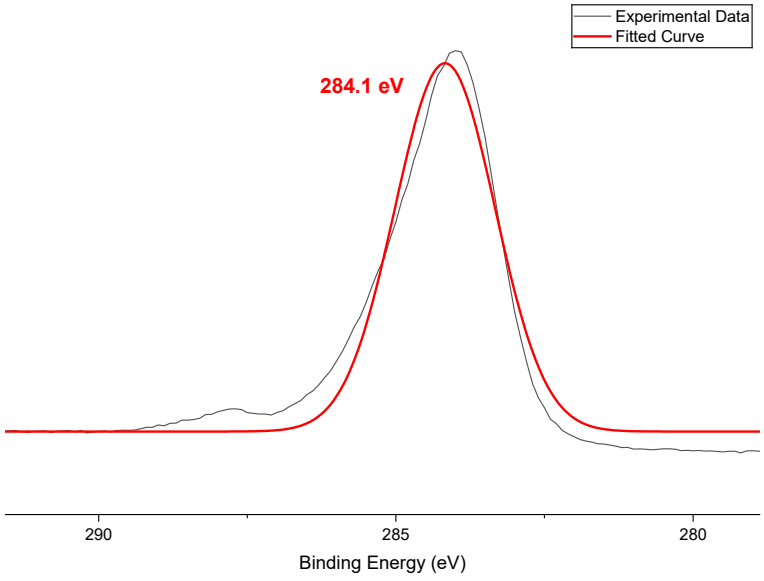

Figure S15. XPS plot of C for complex [Mo(V)(O)(LS^{2-})($LS^{\bullet-}$)] (**1**).

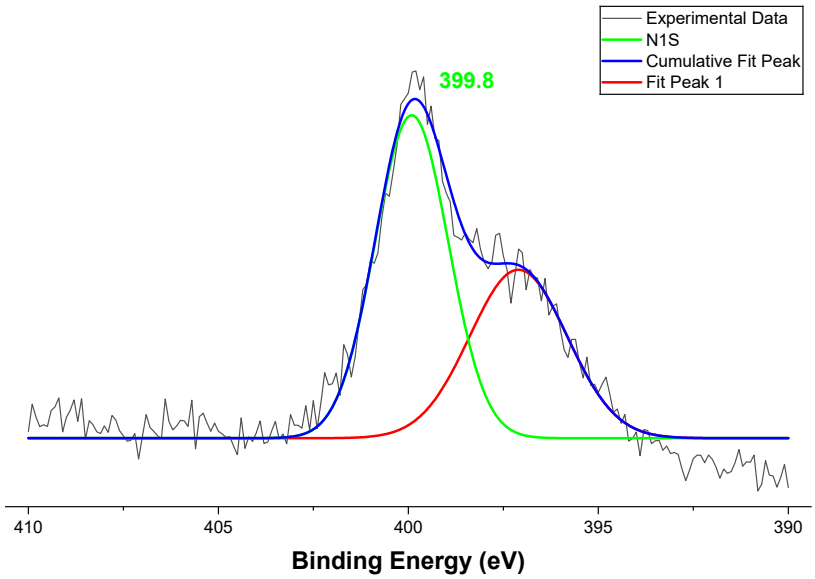

Figure S16. XPS plot of N for complex [Mo(V)(O)(LS^{2-})($LS^{\bullet -}$)] (**1**).

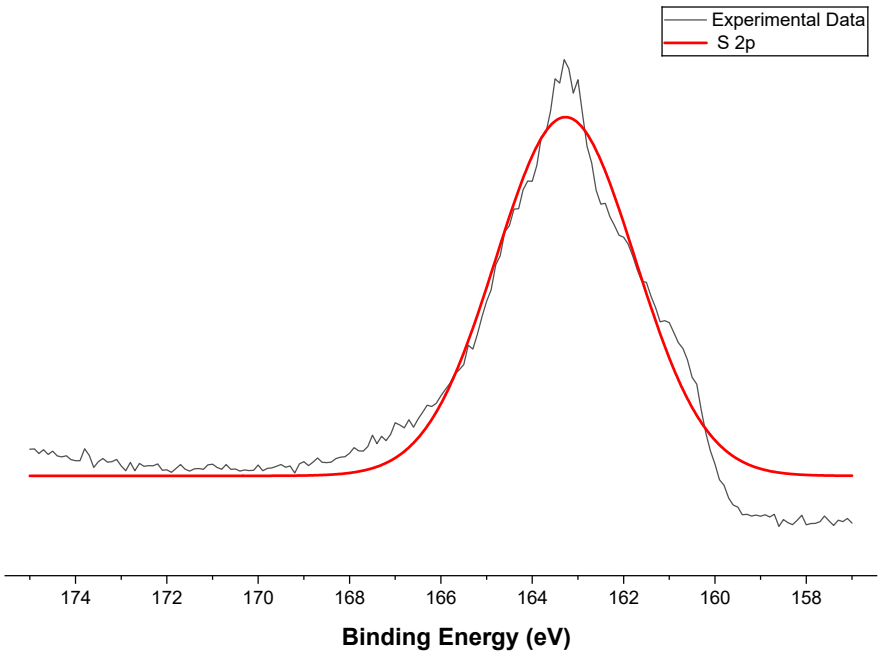

Figure S17. XPS plot of S for complex [Mo(V)(O)(LS^{2-})($LS^{\bullet -}$)] (**1**).

10. Computational Methods

Computational Details

The Dip groups of complexes **1-2** were replaced by Me groups in **1′-2′** for computational cost. Geometry optimisations of the molybdenum-bisdithiolene complexes (**1′-2′**) were carried out using density functional theory (DFT)[S8] employing the meta-GGA M06[S9] functional in conjunction with the def2-TZVPP[S10] basis set. We have replaced the Dipp group with the Me group to save computational time. Although geometry optimisations were performed using multiple density functionals, including B3LYP[S11-S12], BP86[S13], and TPSS[S14], only the M06 functional accurately reproduced the experimentally reported C–C bond lengths of both the radical-anionic and dianionic dithiolene ligands. All the calculations were performed for neutral species (q = 0) considering the possible spin states S = 0 and S = 1, using the Gaussian 16[S15] program package, under gas-phase conditions. It is observed that the singlet-triplet energy gap is negligible across all employed functionals, with calculated values of 1.5 kcal/mol and 0.78 kcal/mol for complexes **1′** and **2′** at the M06/def2-TZVPP level of theory, respectively. The optimised structures correspond to true minima on the potential energy surface, as confirmed by the absence of imaginary vibrational frequencies. Natural Bond Orbital[S16-S17] (NBO) analyses were performed with the NBO 6.0 program at the M06/def2-TZVPP level using the optimised geometries, and Mulliken spin density distributions were subsequently generated.

Table S5. The Singlet-Triplet ($\Delta E_{S\text{-}T}$) energy differences of complex [Mo(V)(O)(LS^{2-})($LS^{\bullet-}$)] (**1**) **were** calculated using different functionals and def2-TZVPP as the basis set.

	B3LYP	BP86	M06
singlet	-3140.6631337	-3140.9562611	-3139.8462023
triplet	-3140.6621424	-3140.9453455	-3139.8437202
Energy difference (kcal/mol)	0.6	6.8	1.5

Table S6. The Singlet-Triplet ($\Delta E_{S\text{-}T}$) energy differences of complex [Mo(V)(O)(LSe^{2-})($LSe^{\bullet-}$)] (**1**) were calculated using different functionals and def2-TZVPP as the basis set.

	B3LYP	BP86	M06	TPSS
singlet	-7147.394689	-7148.116808	-7146.4189971	-7147.3283258
triplet	-7147.3937582	-7148.1042179	-7146.4202352	-7147.3199739
Energy difference (kcal/mol)	0.58	7.9	0.78	5.24

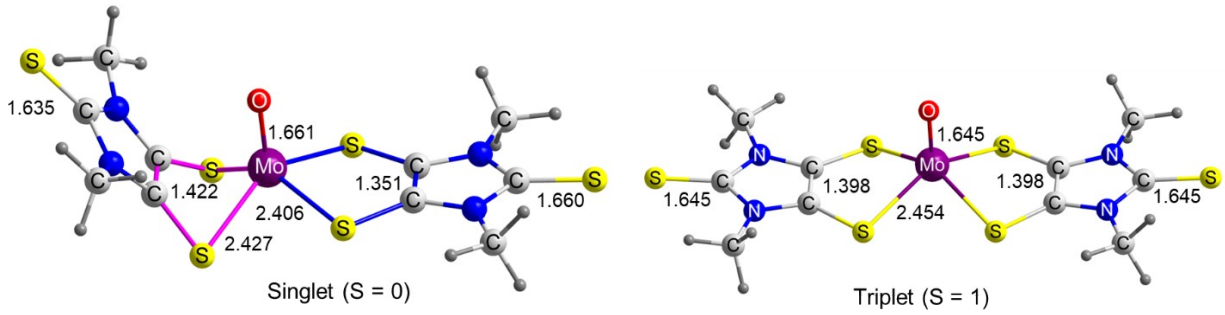

Figure S18. The optimised geometries of complex **1′** at S = 0 and 1 at M06/def2-TZVPP level of theory. The coordination mode involving the radical anionic ligand is denoted by the pink colour, whereas the blue colour represents the coordination of the dianionic ligand. The Bond lengths are given in **Å.**

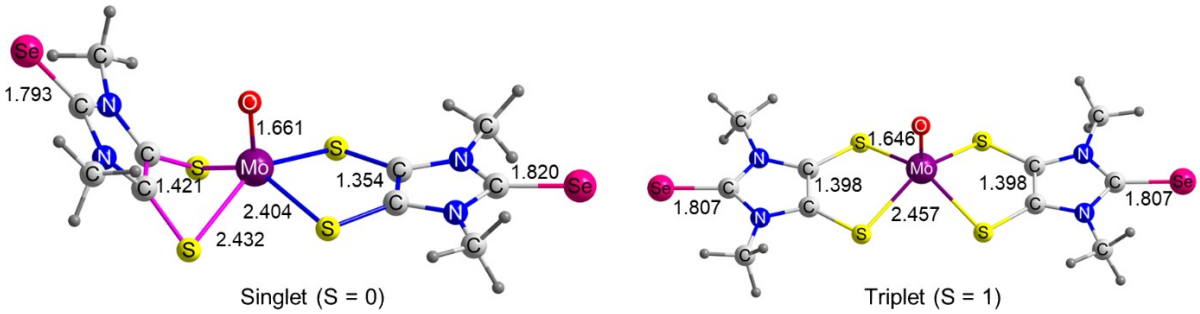

Figure S19. The optimised geometries of complex **2′** at S = 0 and 1 at M06/def2-TZVPP level of theory. The coordination mode involving the radical anionic ligand is denoted by the pink colour, whereas the blue colour represents the coordination of the dianionic ligand. The Bond lengths are given in **Å.**

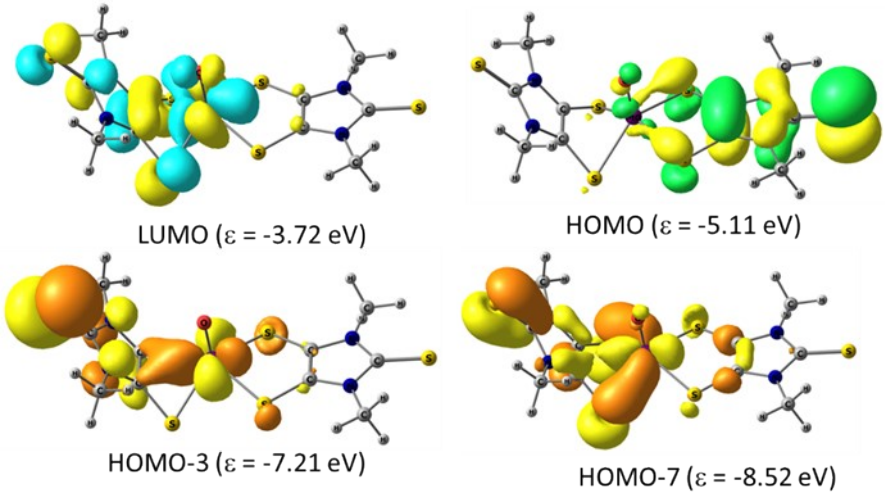

Figure S20. The molecular orbitals of complex **1′** (S = 0) were calculated at the M06/def2-TZVPP level of theory. The LUMOs are visualised using a cyan-yellow colour representation. The orbital localised on the dianionic ligand is shown in a green-yellow colour scheme, while the corresponding orbital on the radical anionic ligand is displayed in orange-yellow.

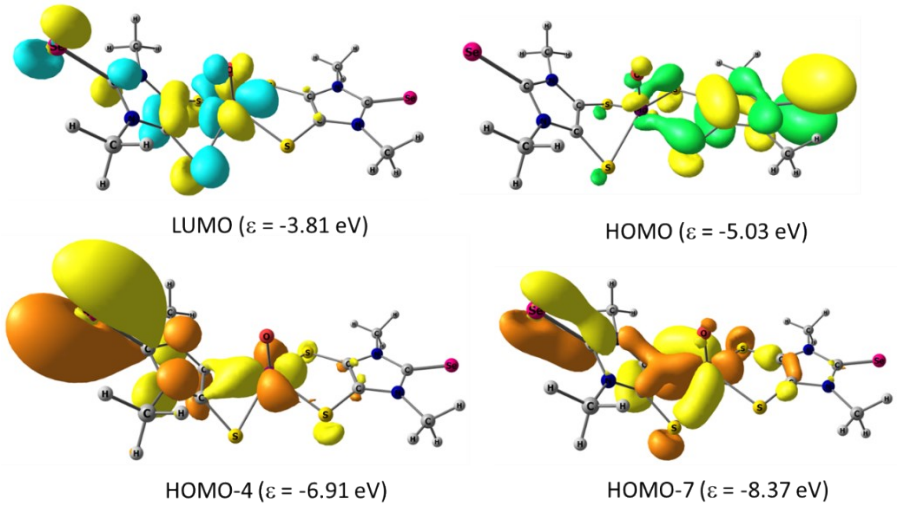

Figure S21. The molecular orbitals of complex **2′** (S = 0) were calculated at the M06/def2-TZVPP level of theory. The LUMOs are visualised using a cyan-yellow colour representation. The orbital localised on the dianionic ligand is shown in a green-yellow colour scheme, while the corresponding orbital on the radical anionic ligand is displayed in orange-yellow.

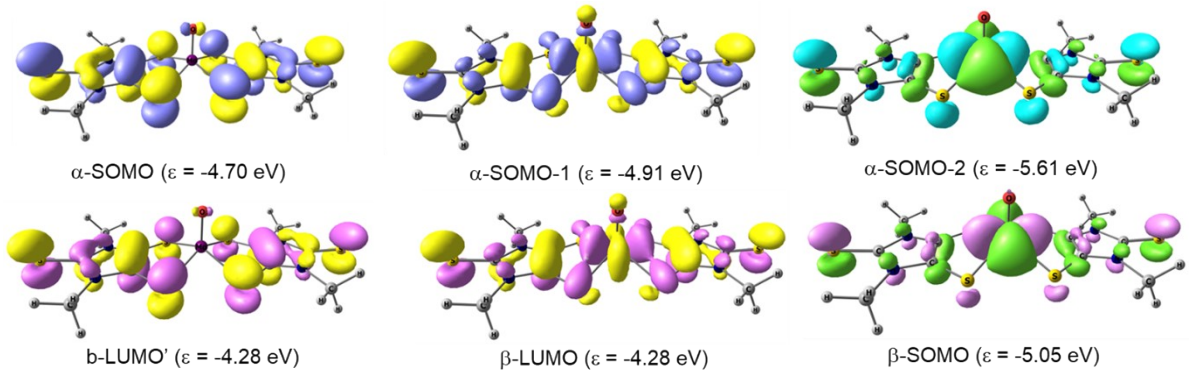

Figure S22. The molecular orbitals of complex **1′** (S = 1) were calculated at the M06/def2-TZVPP level of theory. The α-orbitals containing the unpaired electrons are shown in lavender-yellow, while the corresponding β-LUMOs are displayed in pink-yellow. The matching α-SOMO–2 and β-SOMO are illustrated using cyan-green and rose-green colours, respectively.

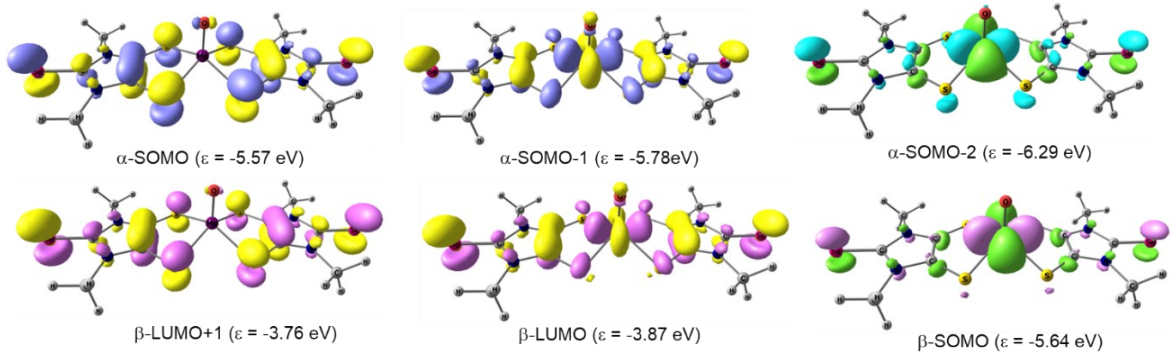

Figure S23. The molecular orbitals of complex **2′** (S = 1) were calculated at the M06/def2-TZVPP level of theory. The α-orbitals containing the unpaired electrons are shown in lavender-yellow, while the

corresponding β-LUMOs are displayed in pink-yellow. The matching α-SOMO–2 and β-SOMO are illustrated using cyan-green and rose-green colours, respectively.

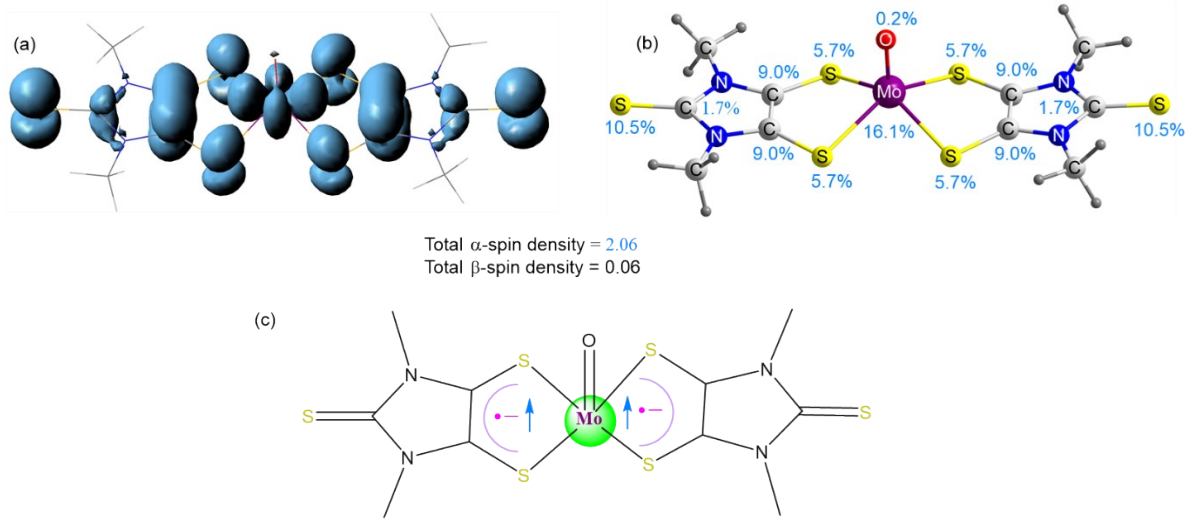

Figure S24. Spin density plot (a) of complex **1′** (S = 1) computed at the M06/def2-TZVPP level of theory. The α-spin density is shown in blue at an isosurface value of 0.003 a.u. The corresponding percentage distribution of α-spin density and electronic spin population representation is also displayed in (b) and (c).

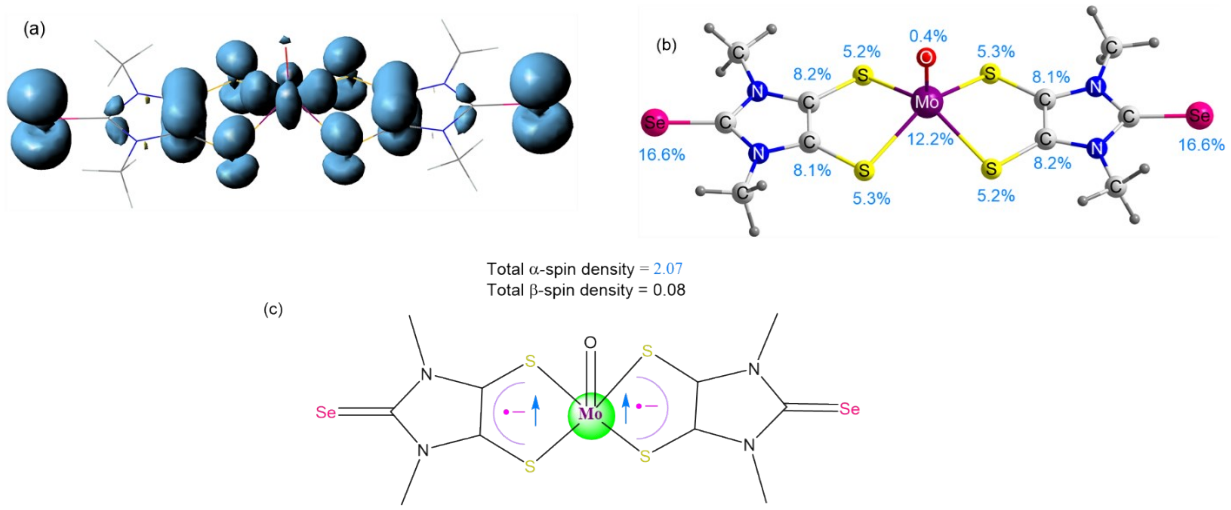

Figure S25. Spin density plot (a) of complex **2′** (S = 1) computed at the M06/def2-TZVPP level of theory. The α-spin density is shown in blue at an isosurface value of 0.003 a.u. The corresponding percentage distribution of α-spin density and electronic spin population representation are also displayed in (b) and (c).

DFT calculation showed that singlet (Figure S21) is the ground stat state for complex **1-2** while singlet diradical and triplet diradical state (Figures S22-S23) are low lying. The corresponding spin densities at triplets state were shown in Figure S24-S25 which is equally distributed to the both side of MoO unit in the ligand part which differ from experimental geometry of the molecules of **1/2**. The optimized geometry of experimentally isolated complexes closely matches with that of singlets state of complexes **1** and **2**. Thus,

we have carried out additional calculations on singlet diradical state. The Dip groups of the ligand has been replaced my Me groups in **1′** and **2′**.

Further, to analyze the open-shell singlet energy and diradical character (*y*) for **1′** and **2′** we performed a fragment-based broken-symmetry DFT (BS-DFT) optimization, in which the metal was placed in one fragment and both the ligands in another. The BS-DFT is a spin-unrestricted DFT approach, where the Kohn–Sham determinant is allowed to break spin symmetry (i.e., allows different spatial orbitals for α and β electrons). The value of $\langle \hat{S}^2 \rangle$ for a closed-shell singlet is 0 and for triplet it is 2. However, in the case of open-shell singlet the expected $\langle \hat{S}^2 \rangle = 1$ is not a pure spin state rather an approximate mixture of singlet and triplet.[S18]

The M06/def2-TZVPP level of theory was used for the BS-DFT optimization which was carried out in ORCA5. RIJCOSX and SlowConv criteria were used in the calculation to aid computational time. Frequency calculations were carried out after BS-DFT optimization. For the first complex (**1′**), reported structure has an imaginary frequency of −49.84 cm^{-1}. The report structure of the second complex (**2′**) also has an imaginary frequency of −42.76 cm^{-1}. These small imaginary frequencies could not be eliminated.

The diradical character (*y*)[S19,S20] was quantified using the occupation number of the highest occupied natural orbital (HONO) and the lowest unoccupied natural orbital (LUNO), obtained from BS-DFT calculations based on **Unrestricted Kohn-Sham** (UKS) based natural orbital analysis.

$$y = 1 - \frac{2T}{1 + T^2}$$

Where T is the orbital overlap parameter calculated from the occupation numbers of the UHF natural orbitals.

$$T = \frac{n_{HOMO} - n_{LUMO}}{2}$$

In general, the diradical index (*y*) describes the extent of bond instability. For closed-shell singlet systems, the *y* value is 0 and for a pure diradical it is expected to be 1.

	HONO	**LUNO**
1'	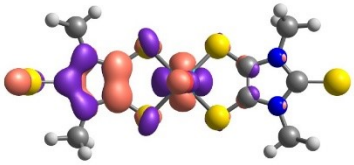	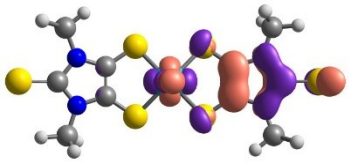
	n_H = 1.07644	n_L = 0.92356
2'	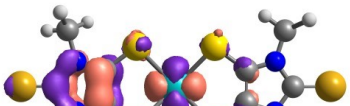	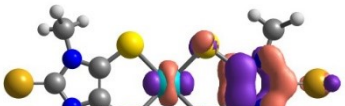

Table S7. The energy differences between Singlet, Triplet and BS-Singlet of complexes [Mo(V)(O)(LS^{2-})($LS^{\bullet-}$)] (1') and [Mo(V)(O)(LSe^{2-})($LSe^{\bullet-}$)] (2') are calculated using M06/def2-TZVPP level of theory.

	1′	**2′**
$E_{Triplet}$ (Hartree)	-3139.8437202	-7146.4202352
$E_{Singlet}$ (Hartree)	-3139.8462023	-7146.4189971
E_{BS} (Hartree)	-3139.8400344	-7146.4168083
E_{S-T} (Kcal/mol)	-1.56	0.78
E_{BS-T} (Kcal/mol)	2.31	2.15
E_{BS-S} (Kcal/mol)	3.87	1.37

Table S8. The open-shell singlet energy (E_{BS}), expected $\langle S^2 \rangle$ value, natural orbitals occupation numbers and the diradical character (y) of complexes [Mo(V)(O)(LS^{2-})($LS^{\bullet-}$)] (**1′**) and [Mo(V)(O)(LSe^{2-})($LSe^{\bullet-}$)] (**2′**) are calculated using M06/def2-TZVPP level of theory.

	E_{BS}	$\langle S^2 \rangle$	HONO	LUNO	y
1′	-3139.8400344Eh	1.0042	1.07644	0.92356	0.84
2′	-7146.4168083Eh	1.0145	1.09871	0.90129	0.80

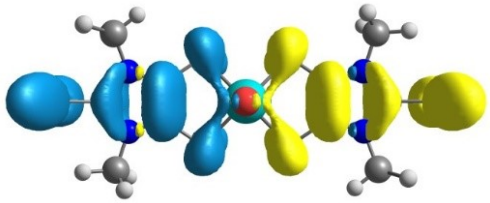

Figure S26. Open-shell singlet Spin density plot of complexes **1′** computed at the M06/def2-TZVPP level of theory with isosurface 0.0015 a.u., where blue colour is shown as α-spin density and yellow colour shown as β-spin density with a metal spin density of 0.002785 and ligand spin density of -0.002785.

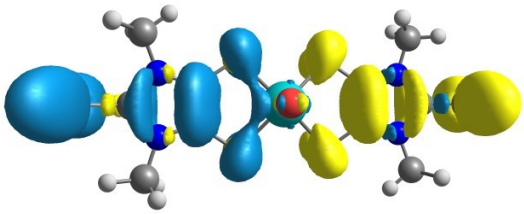

Figure S27. Open-shell singlet Spin density plot of complexes **2′** computed at the M06/def2-TZVPP level of theory with isosurface 0.0015 a.u., where blue colour is shown as α-spin density and yellow colour shown as β-spin density with a metal spin density of 0.019997 and ligand spin density of -0.019997.

11. NMR Spectra:

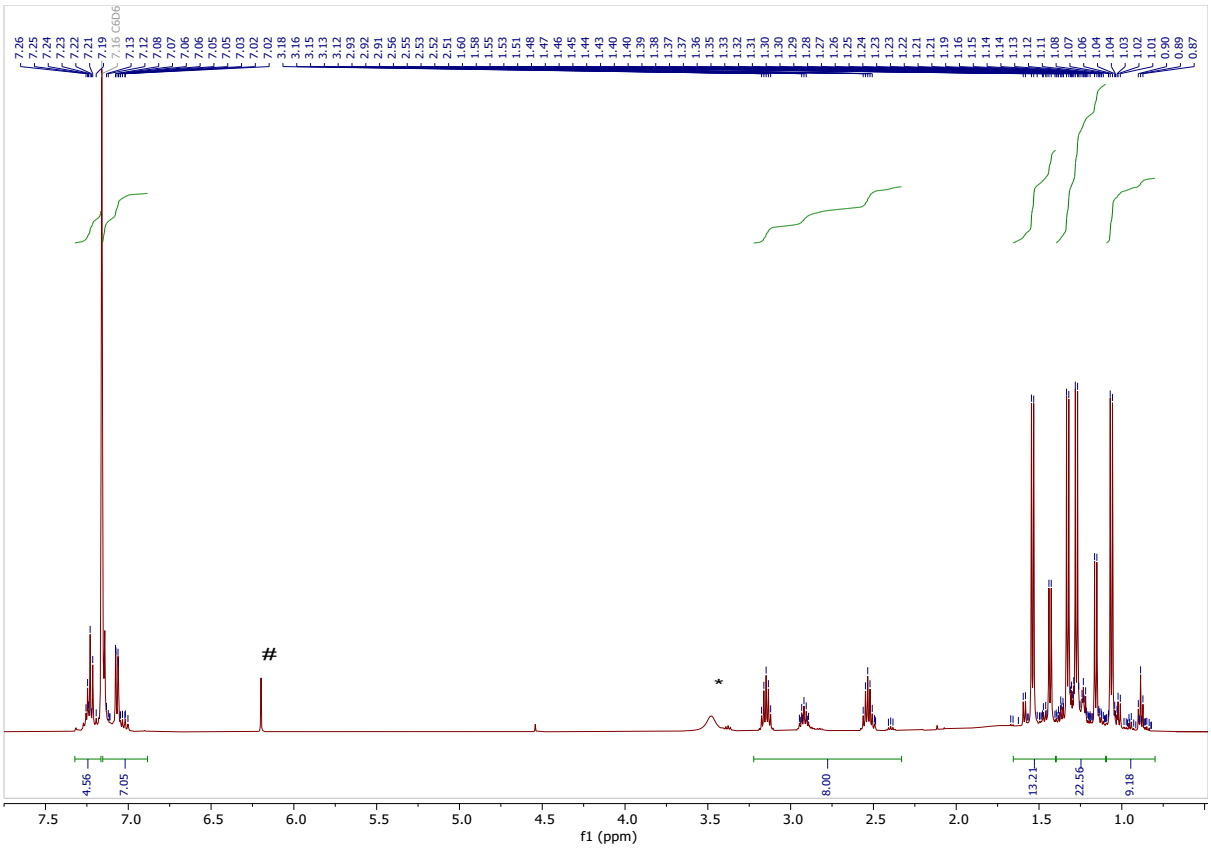

Figure S28. ^{1}H NMR spectrum of complex **1** in C_6D_6 at room temperature (500 MHz) [*: solvent impurity #: impurity].

^{1}H NMR (500 MHz, C_6D_6) δ (ppm): 7.36 – 7.17 (m, 5H), 7.15 – 6.95 (m, 7H), 3.15 (p, J = 6.8 Hz, 2H), 2.92 (p, J = 7.0 Hz, 3H), 2.60 – 2.35 (m, 3H), 1.49 (dd, J = 53.5, 6.8 Hz, 15H), 1.30 (dd, J = 29.9, 6.8 Hz, 18H), 1.18 – 0.72 (m, 15H).

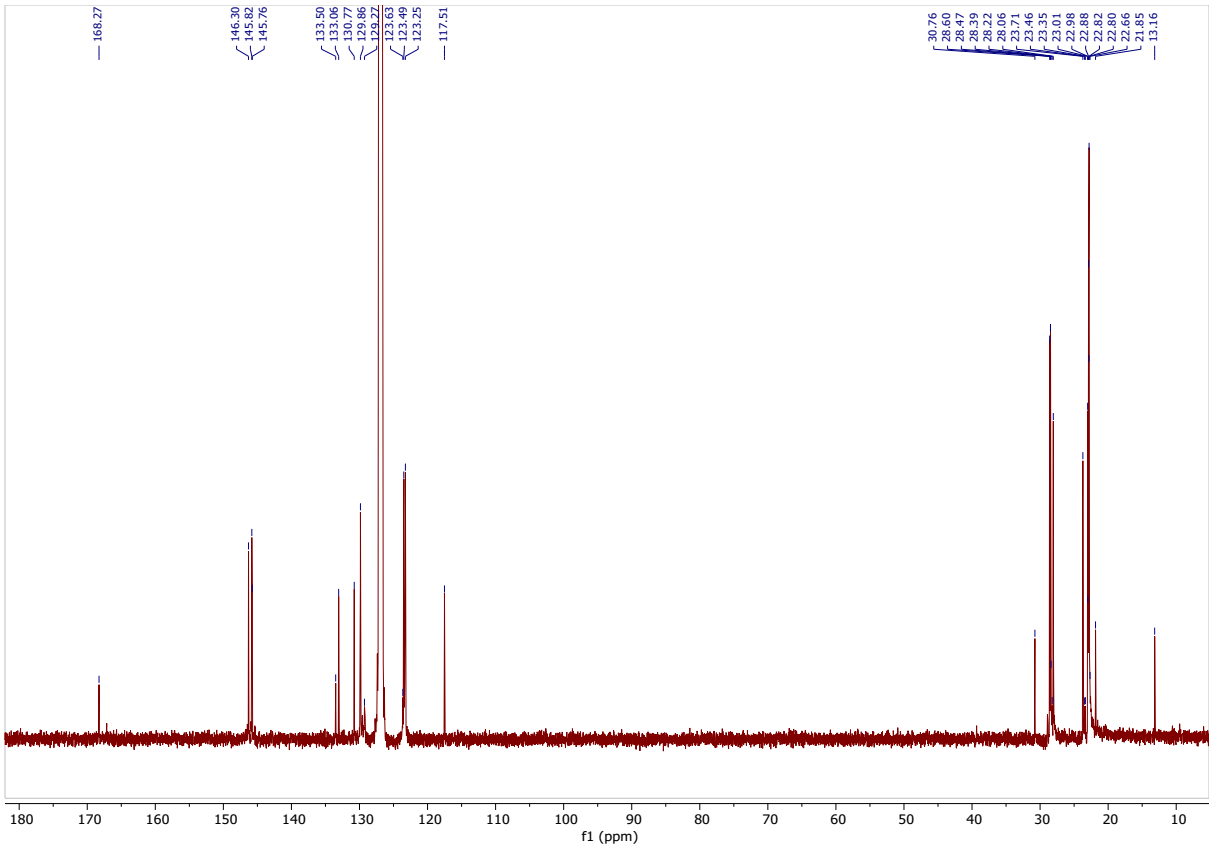

Figure S29. ^{13}C NMR spectrum of complex **1** in C_6D_6 at room temperature (500 MHz, 5000 scans).

^{13}C NMR (500MHz, C_6D_6) δ (ppm): 168.27, 146.30, 145.82, 145.76, 133.50, 133.06, 130.77, 129.86, 129.27, 123.63, 123.49, 123.25, 117.51, 30.76, 28.60, 28.47, 28.39, 28.22, 28.06, 23.71, 23.35, 23.01, 22.98, 22.88, 22.82, 22.80, 21.85, 13.16.

VT-NMR of Complex 1:

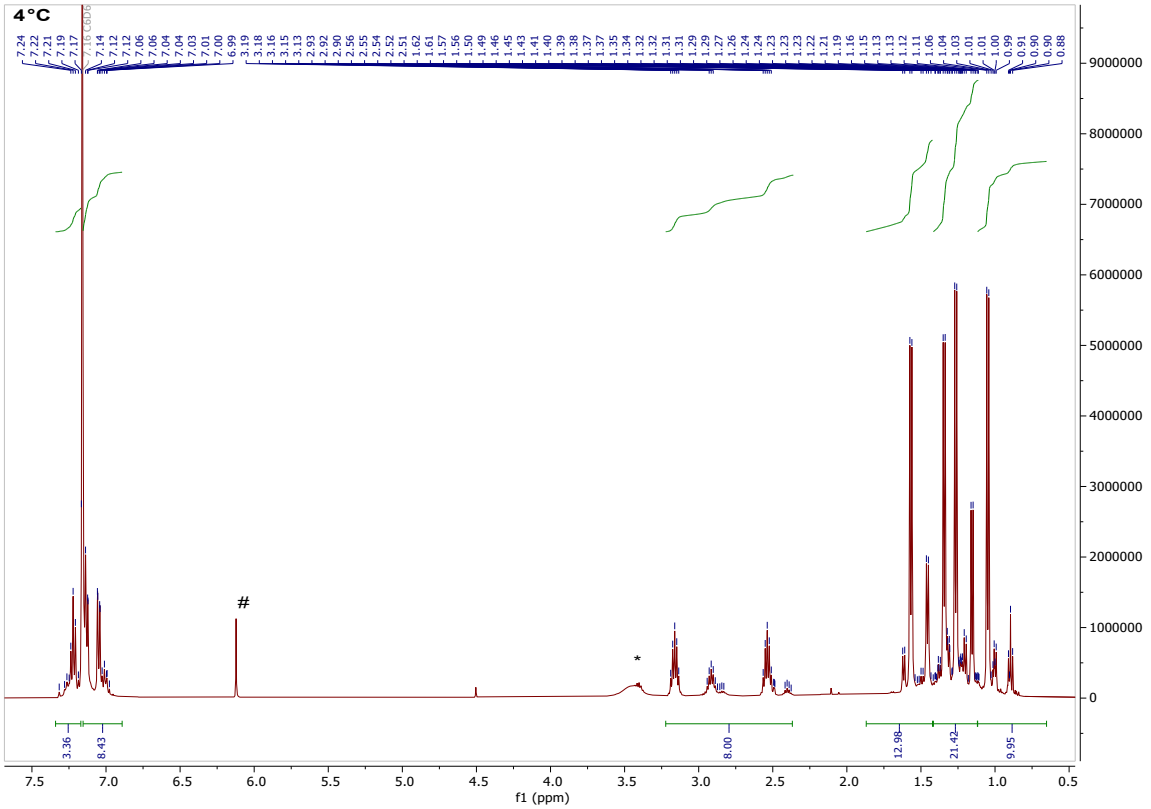

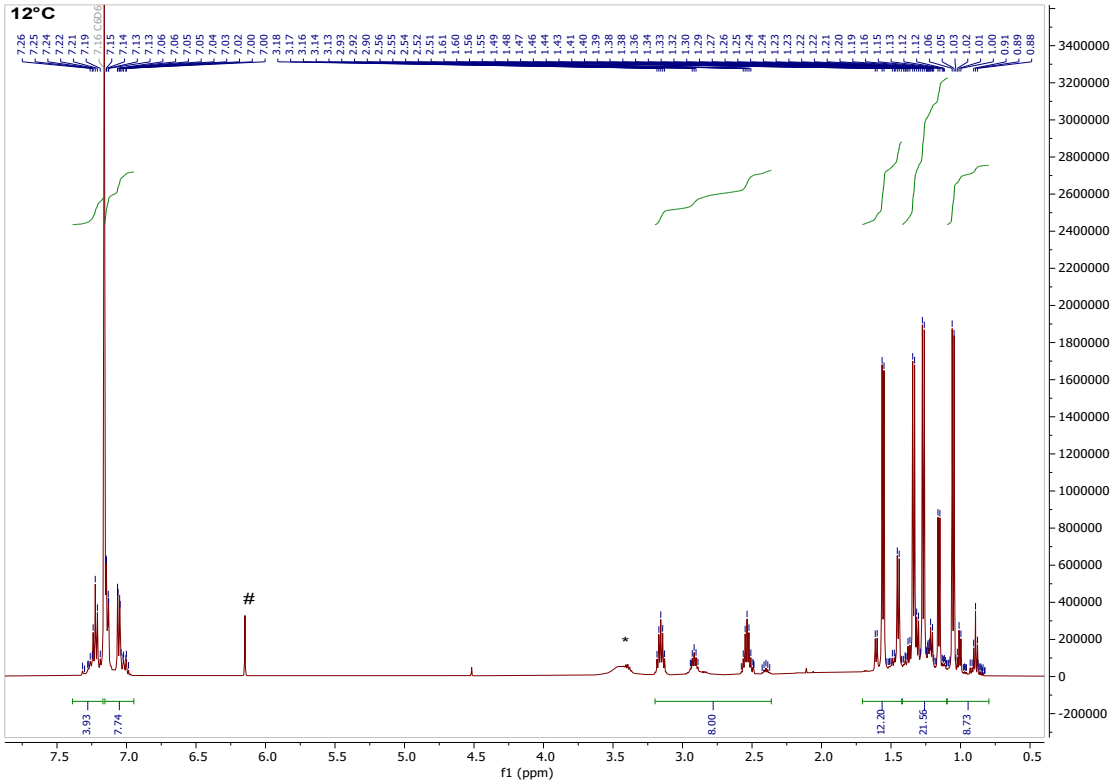

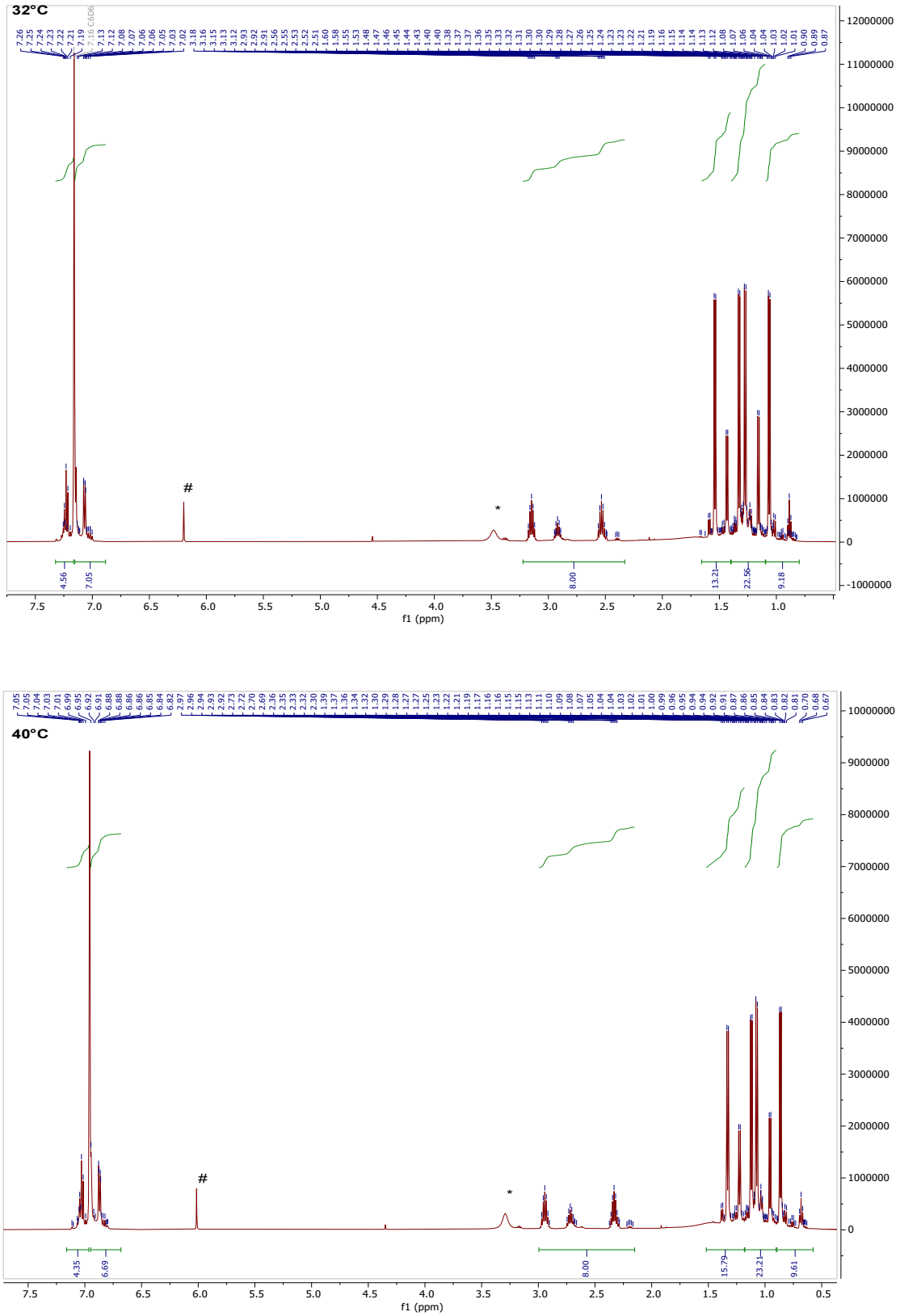

Figure S30. ^{1}H NMR spectrum of complex **1** in C_6D_6 at variable temperature (4 °C, 12 °C, 32 °C and 40 °C**)** (500 MHz) [*: solvent impurity #: impurity].

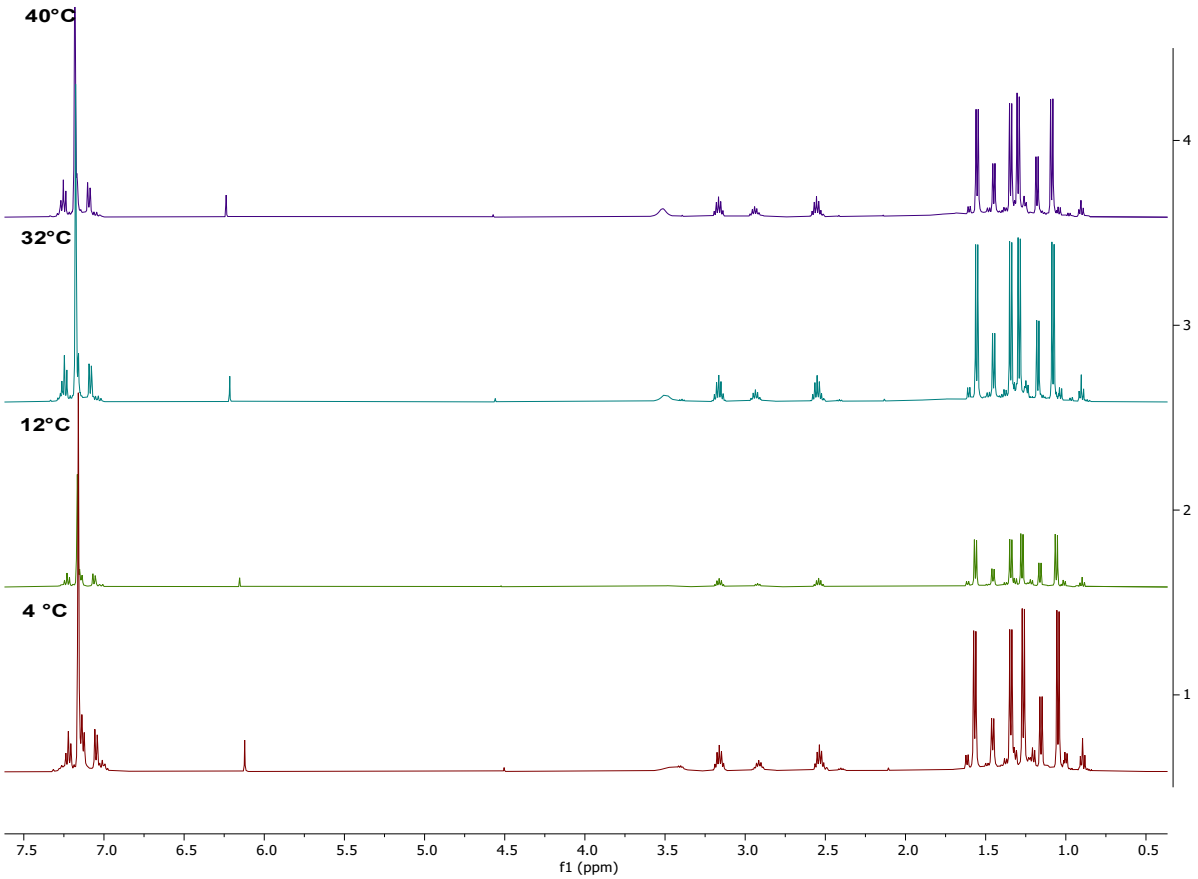

Figure S31. ^{1}H NMR spectrum of complex **1** in C_6D_6 at variable temperature (4 °C, 12 °C, 32 °C and 40 °C) (500 MHz).

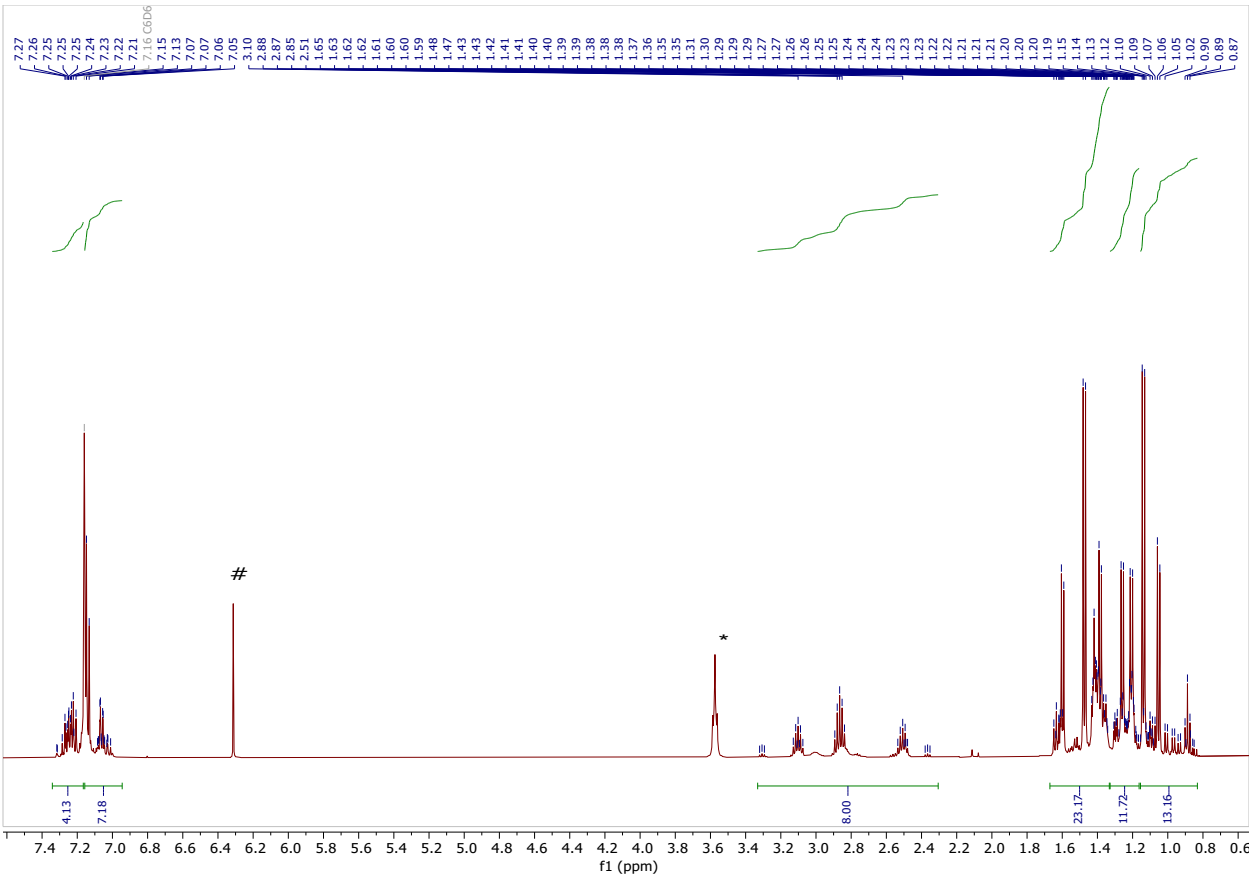

Figure S32. ^{1}H NMR spectrum of complex **2** in C_6D_6 at room temperature (500 MHz) [*: solvent impurity, #: impurity].

^{1}H NMR (500 MHz, C_6D_6) δ (ppm): 7.34 – 7.17 (m, 4H), 7.16 – 6.94 (m, 7H), 3.33 – 2.31 (m, 8H), 1.67 – 1.33 (m, 23H), 1.33 – 1.16 (m, 12H), 1.16 – 0.83 (m, 13H).

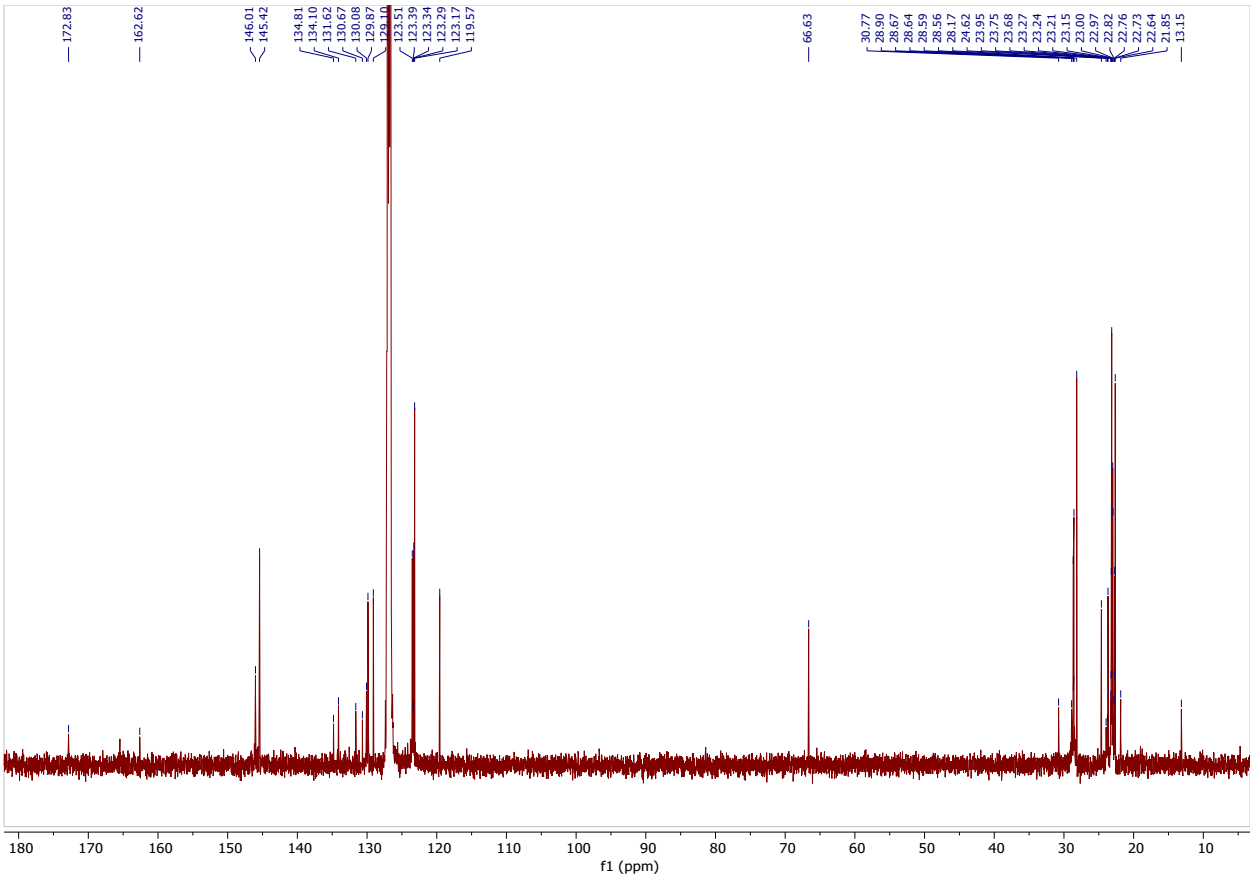

Figure S33. ^{13}C NMR spectrum of complex **2** in C_6D_6 at room temperature (500 MHz, 5000 scans).

^{13}C NMR (500 MHz, C_6D_6) δ (ppm): 172.83, 146.01, 145.42, 134.81, 134.10, 131.62, 130.67, 130.08, 129.87, 129.10, 123.51, 123.39, 123.34, 123.29, 123.17, 119.57, 66.63, 30.77, 28.90, 28.67, 28.59, 28.56, 28.17, 24.62, 23.95, 23.75, 23.68, 23.27, 23.24, 23.21, 23.15, 23.00, 22.97, 22.82, 22.76, 22.73, 22.64, 21.85, 13.15.

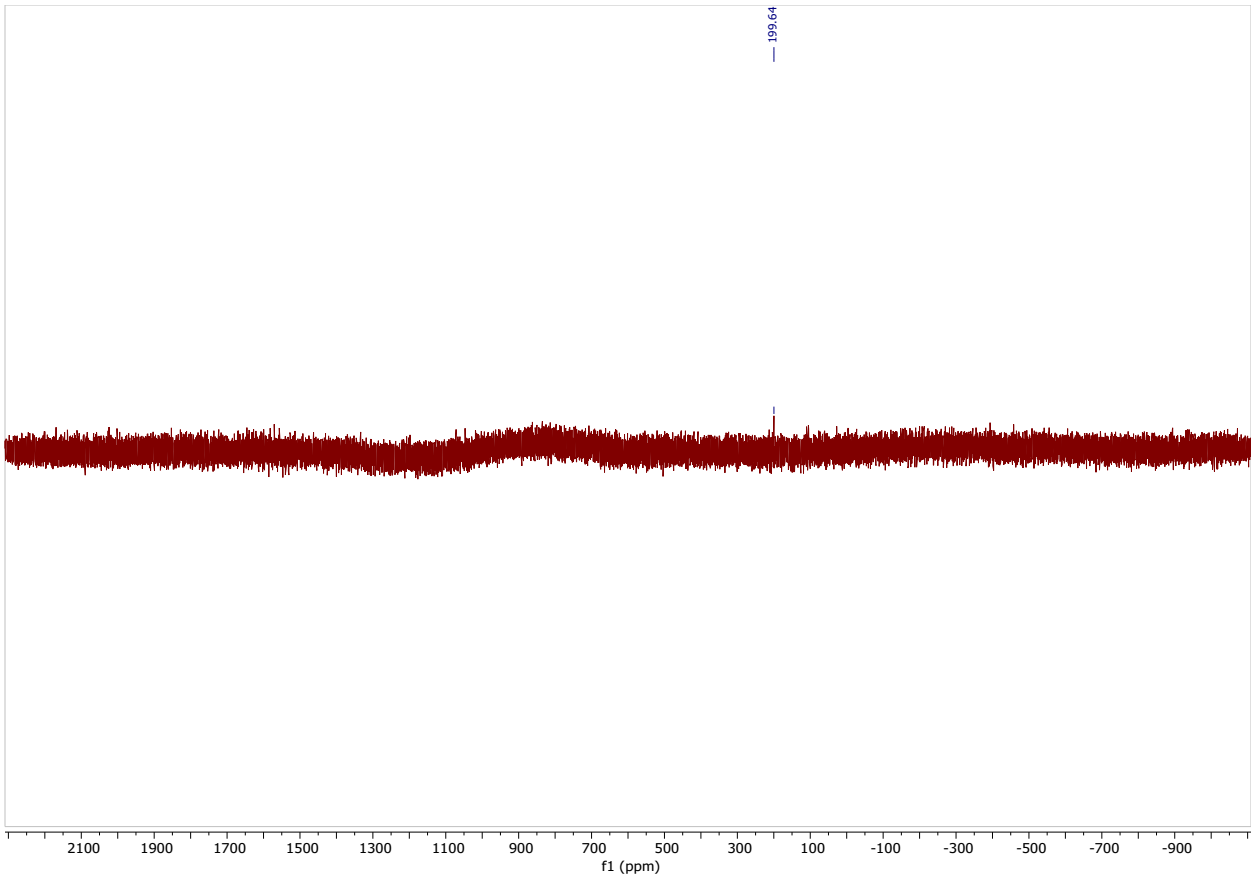

Figure S34. ^{77}Se NMR spectrum of complex **2** in C_6D_6 at room temperature (500 MHz, 1000 scans).

12. Optimised Coordinates

Optimised coordinates of complexes at
M06/def2-TZVPP level of theory.
Energies are in Hartree (hf)

Complex **1′**, Singlet (S = 0)
E = -3139.8462023

42	-0.405696000	-0.003191000	-0.155009000
16	6.467683000	-0.000872000	0.709682000
16	-5.645168000	0.000024000	1.615104000
8	-0.793255000	-0.015506000	1.460988000
7	4.012400000	1.104602000	0.242265000
7	4.027021000	-1.078724000	0.236433000

7	-3.719504000	1.090311000	0.074435000
7	-3.697845000	-1.108034000	0.078261000
6	4.837069000	0.016401000	0.396058000
6	2.730296000	-0.672186000	-0.014290000
6	2.723527000	0.679360000	-0.009507000
6	-2.690815000	-0.710111000	-0.757142000
6	-2.701911000	0.712488000	-0.759445000
6	-4.365881000	-0.013684000	0.596737000
16	-1.522744000	1.705787000	-1.476517000
16	1.331008000	1.652799000	-0.333218000
16	-1.516979000	-1.708421000	-1.477132000
16	1.340787000	-1.646387000	-0.351620000
6	4.431449000	2.478410000	0.328712000
1	5.476014000	2.487032000	0.634720000
1	4.332323000	2.974208000	-0.638166000
1	3.825229000	3.010140000	1.062999000
6	4.503184000	-2.434801000	0.326153000
1	3.650027000	-3.108618000	0.276552000
1	5.192587000	-2.653730000	-0.489889000
1	5.036249000	-2.578844000	1.265568000
6	-3.946849000	-2.479174000	0.458336000
1	-4.800156000	-2.486952000	1.131847000
1	-4.163402000	-3.082229000	-0.421946000
1	-3.069967000	-2.884740000	0.964723000
6	-4.065010000	2.444759000	0.440086000
1	-3.324430000	3.115506000	0.011900000
1	-5.056487000	2.694918000	0.064700000
1	-4.070954000	2.538638000	1.524735000

Complex **1′**, Triplet (S = 1)
E = -3139.8437202

42	-0.000028000	0.000217000	0.422155000
16	6.790971000	-0.003733000	0.011384000

16	-6.790934000	0.003233000	0.011424000
8	0.000021000	0.000224000	2.067827000
7	4.305516000	1.102819000	-0.133270000
7	4.316099000	-1.089063000	-0.122189000
7	-4.316241000	1.088874000	-0.122265000
7	-4.305342000	-1.103016000	-0.133257000
6	5.148075000	0.009821000	-0.076763000
6	3.011081000	-0.700337000	-0.217071000
6	3.006785000	0.698229000	-0.221397000
6	-3.006683000	-0.698235000	-0.221441000
6	-3.011147000	0.700326000	-0.217206000
6	-5.148036000	-0.010116000	-0.076783000
16	-1.620142000	1.683049000	-0.329004000
16	1.618996000	1.683969000	-0.331472000
16	-1.618738000	-1.683751000	-0.331476000
16	1.619942000	-1.682847000	-0.328976000
6	4.735643000	2.480319000	-0.117820000
1	5.809237000	2.496050000	0.053134000
1	4.507208000	2.958125000	-1.070512000
1	4.219430000	3.016290000	0.678048000
6	4.797208000	-2.450292000	-0.094471000
1	3.945331000	-3.112284000	0.042076000
1	5.307553000	-2.692819000	-1.026321000
1	5.502098000	-2.570443000	0.725930000
6	-4.735294000	-2.480566000	-0.117701000
1	-5.808445000	-2.496560000	0.055996000
1	-4.509351000	-2.957757000	-1.071305000
1	-4.216865000	-3.016935000	0.676450000
6	-4.797683000	2.449990000	-0.094556000
1	-3.945793000	3.112249000	0.040580000
1	-5.309308000	2.691898000	-1.025859000
1	-5.501545000	2.570434000	0.726690000

Complex **2′**, Singlet (S = 0)
E = -7146.4189971

42	0.451074000	0.008715000	-0.347239000
8	0.870636000	0.010346000	1.259735000
7	-3.949842000	-1.096866000	0.172593000
7	-3.956843000	1.082800000	0.173001000
7	3.769021000	-1.088381000	-0.178361000
7	3.749594000	1.106323000	-0.155034000
6	-4.754476000	-0.009636000	0.358986000
6	-2.673489000	0.674085000	-0.132840000
6	-2.669114000	-0.679884000	-0.132871000
6	2.729337000	0.717977000	-0.980384000
6	2.738745000	-0.703248000	-0.995198000
6	4.418011000	0.008892000	0.340161000
16	1.549723000	-1.688646000	-1.707955000
16	-1.284741000	-1.649008000	-0.507137000
16	1.547682000	1.723120000	-1.678738000
16	-1.295782000	1.652563000	-0.508183000
6	-4.405392000	-2.460023000	0.280065000
1	-4.915675000	-2.603495000	1.232047000
1	-5.110094000	-2.691235000	-0.519291000
1	-3.544086000	-3.121985000	0.215047000
6	-4.421641000	2.442911000	0.279438000
1	-3.565055000	3.110754000	0.212397000
1	-5.129062000	2.668151000	-0.519231000
1	-4.931609000	2.584119000	1.231924000
6	4.001564000	2.477617000	0.227120000
1	4.867224000	2.488234000	0.884821000
1	4.197881000	3.083842000	-0.655602000
1	3.131604000	2.875943000	0.750756000
6	4.113932000	-2.450155000	0.163596000
1	3.372793000	-3.111977000	-0.277285000

1	5.105688000	-2.692667000	-0.215904000
1	4.119448000	-2.563166000	1.246544000
34	-6.529206000	-0.015316000	0.764876000
34	5.837214000	-0.020629000	1.435663000

Complex **2′**, Triplet (S = 1)
E = -7146.4202352

42	-0.000206000	-0.000230000	0.515141000
8	-0.000297000	-0.000271000	2.160793000
7	-4.316846000	-1.101427000	-0.156822000
7	-4.329291000	1.084463000	-0.147778000
7	4.329510000	-1.084396000	-0.147574000
7	4.316823000	1.101503000	-0.156758000
6	-5.153812000	-0.012149000	-0.137273000
6	-3.020372000	0.698772000	-0.183030000
6	-3.015220000	-0.699099000	-0.186349000
6	3.015238000	0.699029000	-0.185714000
6	3.020558000	-0.698841000	-0.182417000
6	5.153919000	0.012327000	-0.137307000
16	1.625785000	-1.682829000	-0.232805000
16	-1.623470000	-1.685748000	-0.234447000
16	1.623482000	1.685596000	-0.233366000
16	-1.625436000	1.682565000	-0.233574000
6	-4.736524000	-2.483962000	-0.161022000
1	-5.815638000	-2.514528000	-0.032918000
1	-4.462770000	-2.954987000	-1.104890000
1	-4.244040000	-3.014740000	0.652892000
6	-4.800540000	2.451362000	-0.143034000
1	-3.948092000	3.104625000	0.027527000
1	-5.267538000	2.694977000	-1.096794000
1	-5.537567000	2.580728000	0.646928000
6	4.736135000	2.484166000	-0.160506000
1	5.815936000	2.514730000	-0.038394000

1	4.456756000	2.956814000	-1.101897000
1	4.248169000	3.013358000	0.657182000
6	4.800740000	-2.451309000	-0.142601000
1	3.948595000	-3.104427000	0.030045000
1	5.265921000	-2.695780000	-1.097032000
1	5.539222000	-2.579945000	0.646112000
34	-6.960823000	0.002945000	-0.120150000
34	6.960947000	-0.002507000	-0.120611000

Optimised coordinates of Complexes at B3LYP-D3(BJ)/def2-TZVPP level of theory.

Complex **1′**, Singlet (S = 0)
E = -3140.6631337

42	-0.108688000	-0.000022000	0.981111000
16	6.519245000	0.000059000	-1.249962000
16	-6.586679000	0.000342000	-0.826802000
8	-0.638770000	0.000159000	2.560866000
7	4.179476000	1.098998000	-0.379492000
7	4.179351000	-1.099014000	-0.379880000
7	-4.115828000	1.099222000	-0.490102000
7	-4.116088000	-1.099130000	-0.489691000
6	4.966913000	0.000007000	-0.678040000
6	2.955434000	-0.694356000	0.095435000
6	2.955522000	0.694306000	0.095720000
6	-2.812464000	-0.700333000	-0.341239000
6	-2.812300000	0.700160000	-0.341503000
6	-4.951237000	0.000127000	-0.600945000
16	-1.412071000	1.669467000	-0.176048000
16	1.643834000	1.653553000	0.603608000
16	-1.412443000	-1.669845000	-0.175419000
16	1.643637000	-1.653665000	0.602945000
6	4.602082000	2.479204000	-0.508761000
1	5.513968000	2.495741000	-1.097175000
1	3.818449000	3.049582000	-1.004078000

1	4.792551000	2.911340000	0.473370000
6	4.601781000	-2.479232000	-0.509590000
1	3.818656000	-3.049136000	-1.006269000
1	5.514363000	-2.495540000	-1.096926000
1	4.790935000	-2.912058000	0.472486000
6	-4.564203000	-2.477070000	-0.549623000
1	-5.612358000	-2.506457000	-0.269176000
1	-4.451446000	-2.872796000	-1.558817000
1	-3.965576000	-3.069117000	0.138632000
6	-4.563757000	2.477211000	-0.550299000
1	-3.963437000	3.069675000	0.136106000
1	-4.453164000	2.872022000	-1.560092000
1	-5.611292000	2.507166000	-0.267595000

Complex **1′**, Triplet (S = 1)
E = -3140.6621424

42	-0.000015000	0.000001000	0.457890000
16	6.824338000	-0.000169000	-0.062605000
16	-6.824318000	0.000109000	-0.062566000
8	0.000027000	-0.000069000	2.119328000
7	4.330267000	1.099266000	-0.151018000
7	4.330182000	-1.099260000	-0.151520000
7	-4.330164000	1.099264000	-0.151653000
7	-4.330244000	-1.099262000	-0.151104000
6	5.173678000	-0.000048000	-0.118122000
6	3.023140000	-0.701586000	-0.215622000
6	3.023202000	0.701725000	-0.215270000
6	-3.023194000	-0.701731000	-0.215408000
6	-3.023141000	0.701597000	-0.215738000
6	-5.173674000	0.000056000	-0.118179000
16	-1.624798000	1.680189000	-0.286198000
16	1.624945000	1.680458000	-0.285353000
16	-1.624928000	-1.680433000	-0.285574000

16	1.624776000	-1.680144000	-0.286233000
6	4.772217000	2.481272000	-0.141106000
1	5.820545000	2.497118000	0.138303000
1	4.649081000	2.923229000	-1.129180000
1	4.175199000	3.039602000	0.576742000
6	4.772084000	-2.481289000	-0.142287000
1	4.650810000	-2.922217000	-1.131056000
1	5.819898000	-2.497522000	0.139024000
1	4.173671000	-3.040298000	0.573856000
6	-4.772248000	-2.481259000	-0.140854000
1	-5.820160000	-2.497142000	0.140108000
1	-4.650663000	-2.923027000	-1.129208000
1	-4.174116000	-3.039716000	0.575956000
6	-4.772072000	2.481305000	-0.142262000
1	-4.174292000	3.040076000	0.574603000
1	-4.649948000	2.922560000	-1.130769000
1	-5.820108000	2.497401000	0.138226000

Complex **2′**, Singlet (S = 0)
E = -7147.394689

42	0.114456000	0.000140000	1.121707000
8	0.661907000	0.000569000	2.694912000
7	-4.187852000	-1.096424000	-0.190140000
7	-4.188096000	1.096225000	-0.189446000
7	4.110392000	-1.096088000	-0.393060000
7	4.109260000	1.097141000	-0.393807000
6	-4.971272000	-0.000109000	-0.477138000
6	-2.958109000	0.693974000	0.274337000
6	-2.957960000	-0.694215000	0.273982000
6	2.805830000	0.699760000	-0.229603000
6	2.806333000	-0.700087000	-0.229108000
6	4.934973000	0.000803000	-0.514290000
16	1.406359000	-1.669585000	-0.049364000

16	-1.642037000	-1.655985000	0.769110000
16	1.405891000	1.669341000	-0.050334000
16	-1.642400000	1.655934000	0.769576000
6	-4.606090000	-2.480105000	-0.313845000
1	-5.497931000	-2.509034000	-0.931694000
1	-3.803210000	-3.053308000	-0.772982000
1	-4.828699000	-2.896549000	0.668094000
6	-4.605966000	2.480027000	-0.312905000
1	-3.807934000	3.051145000	-0.783075000
1	-5.504701000	2.507793000	-0.920727000
1	-4.816676000	2.899690000	0.670269000
6	4.555994000	2.476524000	-0.463272000
1	5.568020000	2.532742000	-0.074506000
1	4.551469000	2.826881000	-1.494931000
1	3.880745000	3.086377000	0.131284000
6	4.561008000	-2.474344000	-0.461552000
1	3.859334000	-3.091500000	0.093253000
1	4.604142000	-2.809785000	-1.497189000
1	5.554453000	-2.537872000	-0.028247000
34	-6.684780000	-0.000465000	-1.083996000
34	6.725932000	-0.000465000	-0.794499000

Complex **2′**, Triplet (S = 1)
E = -7147 .3937582

42	-0.000090000	-0.000004000	0.463101000
8	-0.000418000	-0.000014000	2.124644000
7	-4.330430000	-1.096330000	-0.140683000
7	-4.330322000	1.096508000	-0.140949000
7	4.330421000	-1.096460000	-0.140895000
7	4.330477000	1.096382000	-0.140843000
6	-5.165736000	0.000119000	-0.107182000
6	-3.021326000	0.700607000	-0.208650000
6	-3.021369000	-0.700583000	-0.208582000

6	3.021435000	0.700592000	-0.208317000
6	3.021407000	-0.700593000	-0.208326000
6	5.165836000	-0.000059000	-0.107279000
16	1.622742000	-1.680849000	-0.281939000
16	-1.622614000	-1.680749000	-0.282579000
16	1.622751000	1.680827000	-0.281993000
16	-1.622612000	1.680815000	-0.282486000
6	-4.766240000	-2.481710000	-0.133169000
1	-5.797952000	-2.511848000	0.201203000
1	-4.694149000	-2.903440000	-1.134915000
1	-4.126033000	-3.046534000	0.540529000
6	-4.765626000	2.482038000	-0.133184000
1	-4.683905000	2.906651000	-1.132955000
1	-5.800364000	2.511334000	0.191769000
1	-4.131688000	3.044855000	0.548136000
6	4.765865000	2.481895000	-0.133077000
1	5.800285000	2.511274000	0.192875000
1	4.685173000	2.906201000	-1.133062000
1	4.131239000	3.044928000	0.547419000
6	4.765640000	-2.482025000	-0.133141000
1	4.133310000	-3.044394000	0.550058000
1	4.681473000	-2.907273000	-1.132428000
1	5.801126000	-2.511140000	0.189437000
34	-6.979782000	-0.000078000	-0.049678000
34	6.979899000	-0.000022000	-0.049806000

Optimised coordinates of Complexes at BP86-D3(BJ)/def2-TZVPP level of theory.

Complex **1′**, Singlet (S = 0)
E = -3140.9562611

42	-0.122991000	0.000150000	0.954037000
16	6.530049000	-0.000135000	-1.233680000
16	-6.601225000	-0.000182000	-0.747385000
8	-0.682288000	0.000201000	2.541695000

7	4.179440000	1.106007000	-0.353240000
7	4.179490000	-1.106092000	-0.352763000
7	-4.104929000	1.106043000	-0.502057000
7	-4.104703000	-1.106314000	-0.502461000
6	4.974084000	-0.000082000	-0.656401000
6	2.949551000	-0.697641000	0.121756000
6	2.949524000	0.697706000	0.121484000
6	-2.792222000	-0.703746000	-0.389664000
6	-2.792341000	0.703698000	-0.389492000
6	-4.952752000	-0.000193000	-0.584051000
16	-1.377927000	1.671211000	-0.232017000
16	1.621975000	1.654101000	0.625408000
16	-1.377677000	-1.671059000	-0.232048000
16	1.622014000	-1.653885000	0.625982000
6	4.605725000	2.487293000	-0.488551000
1	5.552596000	2.486232000	-1.040388000
1	3.840411000	3.053387000	-1.035324000
1	4.753308000	2.941217000	0.500870000
6	4.605774000	-2.487425000	-0.487586000
1	3.841679000	-3.053257000	-1.036348000
1	5.553899000	-2.486313000	-1.037273000
1	4.750937000	-2.941662000	0.502041000
6	-4.554259000	-2.487573000	-0.535183000
1	-5.636560000	-2.488338000	-0.364338000
1	-4.336400000	-2.940225000	-1.512083000
1	-4.035290000	-3.051554000	0.249998000
6	-4.554888000	2.487177000	-0.534455000
1	-4.030542000	3.052431000	0.246199000
1	-4.343703000	2.938144000	-1.513619000
1	-5.636035000	2.488382000	-0.356527000

Complex **1′**, Triplet (S = 1)
E = -3140.9453455

42	-0.000093000	-0.000139000	0.415252000
16	6.816708000	-0.000020000	0.048830000
16	-6.816653000	0.000317000	0.049080000
8	-0.000232000	-0.000281000	2.095457000
7	4.313106000	1.105829000	-0.132956000
7	4.313039000	-1.105753000	-0.133628000
7	-4.312936000	1.105860000	-0.133743000
7	-4.313149000	-1.105708000	-0.133227000
6	5.162108000	0.000003000	-0.068403000
6	3.001296000	-0.702523000	-0.241195000
6	3.001312000	0.702762000	-0.240760000
6	-3.001348000	-0.702730000	-0.241197000
6	-3.001219000	0.702558000	-0.241560000
6	-5.162054000	0.000173000	-0.068441000
16	-1.589750000	1.678561000	-0.342532000
16	1.589997000	1.678940000	-0.341424000
16	-1.590037000	-1.679009000	-0.341761000
16	1.589964000	-1.678637000	-0.342364000
6	4.758944000	2.488520000	-0.100600000
1	5.822435000	2.486439000	0.162824000
1	4.620512000	2.956506000	-1.084454000
1	4.174798000	3.039660000	0.647235000
6	4.758721000	-2.488507000	-0.102016000
1	4.617127000	-2.956837000	-1.085246000
1	5.823020000	-2.486376000	0.158168000
1	4.176886000	-3.039356000	0.647848000
6	-4.759036000	-2.488390000	-0.100552000
1	-5.822262000	-2.486242000	0.163956000
1	-4.621729000	-2.956275000	-1.084616000
1	-4.174036000	-3.039623000	0.646542000
6	-4.758523000	2.488658000	-0.101943000

1	-4.175311000	3.039695000	0.646704000
1	-4.618610000	2.956622000	-1.085592000
1	-5.822379000	2.486703000	0.160032000

Complex **2′**, Singlet (S = 0)
E = -7148.116808

42	0.128342000	0.000203000	1.093630000
8	0.704735000	0.000409000	2.674588000
7	-4.187398000	-1.103566000	-0.163419000
7	-4.187494000	1.103485000	-0.163476000
7	4.097061000	-1.103801000	-0.419540000
7	4.097095000	1.103630000	-0.419760000
6	-4.977665000	-0.000078000	-0.455752000
6	-2.951242000	0.697456000	0.299560000
6	-2.951177000	-0.697405000	0.299574000
6	2.784698000	0.703093000	-0.283947000
6	2.784679000	-0.703197000	-0.283785000
6	4.934830000	-0.000107000	-0.517637000
16	1.372318000	-1.671399000	-0.105865000
16	-1.619554000	-1.656749000	0.789115000
16	1.372368000	1.671421000	-0.106304000
16	-1.619687000	1.656924000	0.789058000
6	-4.607996000	-2.488635000	-0.292686000
1	-5.547326000	-2.498332000	-0.857488000
1	-3.830452000	-3.054023000	-0.822188000
1	-4.767147000	-2.932347000	0.699370000
6	-4.608208000	2.488517000	-0.292780000
1	-3.830482000	3.054041000	-0.821869000
1	-5.547289000	2.498164000	-0.857996000
1	-4.767872000	2.932109000	0.699248000
6	4.541450000	2.487488000	-0.465451000
1	5.609402000	2.506877000	-0.220917000
1	4.390210000	2.906575000	-1.469474000

1	3.961156000	3.066845000	0.263079000
6	4.541341000	-2.487690000	-0.464918000
1	3.962183000	-3.066603000	0.264874000
1	4.388591000	-2.907459000	-1.468425000
1	5.609654000	-2.506846000	-0.221941000
34	-6.691970000	-0.000164000	-1.069423000
34	6.738290000	-0.000097000	-0.738259000

Complex **2′**, Triplet (S = 1)
E = -7148.1042179

42	0.084827000	-0.000498000	1.018429000
8	0.538725000	-0.000709000	2.633617000
7	-4.240268000	-1.102883000	-0.149475000
7	-4.240284000	1.103063000	-0.148481000
7	4.176098000	-1.102722000	-0.385075000
7	4.175644000	1.103059000	-0.385344000
6	-5.035177000	0.000213000	-0.427652000
6	-2.998284000	0.701643000	0.293820000
6	-2.998286000	-0.701847000	0.293198000
6	2.864729000	0.701653000	-0.247279000
6	2.865009000	-0.701826000	-0.247113000
6	5.013210000	0.000325000	-0.478159000
16	1.449013000	-1.672383000	-0.097101000
16	-1.659661000	-1.684854000	0.721273000
16	1.448362000	1.671695000	-0.097298000
16	-1.659660000	1.684249000	0.722729000
6	-4.653009000	-2.490536000	-0.289417000
1	-5.647697000	-2.497061000	-0.748879000
1	-3.930947000	-3.022038000	-0.922315000
1	-4.690325000	-2.970972000	0.697020000
6	-4.652969000	2.490838000	-0.287345000
1	-3.931590000	3.022554000	-0.920851000
1	-5.648169000	2.497700000	-0.745697000

1	-4.689057000	2.970814000	0.699356000
6	4.612081000	2.489490000	-0.439756000
1	5.698875000	2.504828000	-0.301694000
1	4.357060000	2.930351000	-1.412705000
1	4.108054000	3.051641000	0.356071000
6	4.613177000	-2.488966000	-0.439163000
1	4.106852000	-3.051718000	0.354768000
1	4.361297000	-2.929286000	-1.413179000
1	5.699552000	-2.504142000	-0.297861000
34	-6.758390000	0.000443000	-1.018510000
34	6.823198000	0.000588000	-0.689986000

Optimised coordinates of Complex 2 at TPSSTPSS-(D3) BJ/def2-TZVPP level of theory.

Complex **2′**, Singlet (S = 0)
E = -7147.3283258

42	0.135730000	-0.000332000	1.040774000
8	0.715821000	-0.000630000	2.618642000
7	-4.204525000	-1.101011000	-0.150638000
7	-4.204503000	1.101218000	-0.150051000
7	4.109522000	-1.101058000	-0.409517000
7	4.109241000	1.101331000	-0.409696000
6	-4.998369000	0.000168000	-0.424684000
6	-2.959833000	0.695260000	0.285188000
6	-2.959849000	-0.695310000	0.284882000
6	2.795803000	0.701650000	-0.301686000
6	2.795971000	-0.701714000	-0.301619000
6	4.946685000	0.000229000	-0.489491000
16	1.385183000	-1.672368000	-0.152887000
16	-1.618684000	-1.653668000	0.742974000

16	1.384776000	1.671965000	-0.152833000
16	-1.618577000	1.653339000	0.743627000
6	-4.632832000	-2.489259000	-0.272949000
1	-5.574121000	-2.491756000	-0.823591000
1	-3.863598000	-3.050132000	-0.808335000
1	-4.778177000	-2.923544000	0.719561000
6	-4.632669000	2.489562000	-0.271764000
1	-3.865608000	3.049783000	-0.810959000
1	-5.576283000	2.491878000	-0.818425000
1	-4.773507000	2.924679000	0.721024000
6	4.558997000	2.488711000	-0.445912000
1	5.613869000	2.501596000	-0.170766000
1	4.435779000	2.897923000	-1.452041000
1	3.957766000	3.063091000	0.261299000
6	4.559658000	-2.488316000	-0.445890000
1	3.957109000	-3.063275000	0.259717000
1	4.438511000	-2.896796000	-1.452569000
1	5.613991000	-2.501303000	-0.168703000
34	-6.723933000	0.000238000	-1.000765000
34	6.752001000	0.000329000	-0.671855000

Complex **2′**, Triplet (S = 1)
E = - 7147.3199739

42	-0.000045000	0.000014000	0.384358000
8	-0.000079000	0.000047000	2.062713000
7	-4.311748000	-1.100586000	-0.134546000
7	-4.311661000	1.100712000	-0.134975000
7	4.311723000	-1.100715000	-0.135125000

7	4.311778000	1.100569000	-0.134623000
6	-5.149472000	0.000091000	-0.064026000
6	-3.000313000	0.699944000	-0.255116000
6	-3.000345000	-0.699975000	-0.254867000
6	3.000359000	0.699938000	-0.254849000
6	3.000331000	-0.699960000	-0.255072000
6	5.149516000	-0.000099000	-0.064159000
16	1.593579000	-1.679467000	-0.369765000
16	-1.593611000	-1.679518000	-0.369603000
16	1.593660000	1.679523000	-0.369518000
16	-1.593526000	1.679404000	-0.369961000
6	-4.754959000	-2.490400000	-0.100226000
1	-5.795662000	-2.494172000	0.224563000
1	-4.672084000	-2.931796000	-1.096556000
1	-4.121920000	-3.041669000	0.597895000
6	-4.754585000	2.490620000	-0.100886000
1	-4.663237000	2.934187000	-1.095491000
1	-5.797894000	2.493803000	0.215476000
1	-4.127345000	3.040289000	0.603731000
6	4.754735000	2.490441000	-0.099844000
1	5.797295000	2.493692000	0.218953000
1	4.665828000	2.933839000	-1.094754000
1	4.125770000	3.040246000	0.603124000
6	4.754459000	-2.490663000	-0.100557000
1	4.130663000	-3.039055000	0.608130000
1	4.658087000	-2.935977000	-1.093890000

1 5.799265000 -2.493391000 0.210854000

34 -6.962188000 -0.000007000 0.076345000

34 6.962280000 0.000021000 0.076223000

Optimised Coordinates

Optimised coordinates of complexes at

M06/def2-TZVPP level of theory

Energies are in Hartree (hf)

Complex **1′**, Triplet (S = 1)

E = -3139.84372027

42 0.000945000 -0.000386000 0.417501000

16 6.791373000 -0.003607000 0.000574000

16 -6.790690000 0.003295000 0.015930000

8 0.003070000 -0.001511000 2.063159000

7 4.305695000 1.102807000 -0.141639000

7 4.316517000 -1.089074000 -0.131334000

7 -4.316141000 1.088988000 -0.119825000

7 -4.305308000 -1.102884000 -0.133060000

6 5.148397000 0.009863000 -0.086218000

6 3.011350000 -0.700456000 -0.224983000

6 3.006931000 0.698105000 -0.228764000

6 -3.006750000 -0.698046000 -0.222468000

6 -3.011179000 0.700521000 -0.216815000

6 -5.147908000 -0.010026000 -0.074379000

16	-1.620314000	1.683297000	-0.329611000
16	1.618945000	1.683778000	-0.337161000
16	-1.619006000	-1.683537000	-0.335324000
16	1.620213000	-1.683068000	-0.336000000
6	4.735693000	2.480343000	-0.126135000
1	5.809438000	2.496115000	0.043882000
1	4.506382000	2.958441000	-1.078472000
1	4.220125000	3.016011000	0.670357000
6	4.797886000	-2.450228000	-0.104336000
1	3.946142000	-3.112419000	0.032067000
1	5.308110000	-2.692220000	-1.036388000
1	5.502954000	-2.570689000	0.715870000
6	-4.735234000	-2.480453000	-0.118448000
1	-5.808622000	-2.496489000	0.053776000
1	-4.507872000	-2.957304000	-1.071877000
1	-4.217993000	-3.017133000	0.676278000
6	-4.797462000	2.450102000	-0.090065000
1	-3.945468000	3.112112000	0.045649000
1	-5.309422000	2.693370000	-1.020834000
1	-5.500998000	2.569426000	0.731618000

Complex **2′**, Triplet (S = 1)

E = -7146.42023526

42	0.000307000	0.000003000	0.514407000
8	-0.001507000	0.001170000	2.160063000
7	-4.315464000	-1.102678000	-0.161848000

7	-4.328562000	1.083202000	-0.153337000
7	4.330690000	-1.084116000	-0.143773000
7	4.317604000	1.101756000	-0.155358000
6	-5.152792000	-0.013660000	-0.143407000
6	-3.019510000	0.697903000	-0.187016000
6	-3.013927000	-0.699978000	-0.189864000
6	3.016121000	0.699017000	-0.184963000
6	3.021701000	-0.698872000	-0.180152000
6	5.154903000	0.012764000	-0.134029000
16	1.627126000	-1.683129000	-0.230485000
16	-1.621897000	-1.686292000	-0.235809000
16	1.624181000	1.685252000	-0.234655000
16	-1.624829000	1.682086000	-0.236354000
6	-4.734569000	-2.485400000	-0.165568000
1	-5.814610000	-2.516002000	-0.045553000
1	-4.453279000	-2.958561000	-1.106124000
1	-4.248231000	-3.014084000	0.653415000
6	-4.800110000	2.450007000	-0.149593000
1	-3.948076000	3.103483000	0.022233000
1	-5.265572000	2.693381000	-1.104163000
1	-5.538446000	2.579304000	0.639153000
6	4.736711000	2.484475000	-0.160313000
1	5.816561000	2.515253000	-0.038641000
1	4.456893000	2.956342000	-1.101957000
1	4.249086000	3.014279000	0.657180000
6	4.802221000	-2.450918000	-0.137397000
1	3.949946000	-3.104142000	0.034191000
1	5.268998000	-2.695680000	-1.090970000
1	5.539462000	-2.579071000	0.652558000
34	-6.959832000	0.000935000	-0.128140000
34	6.961912000	-0.001798000	-0.115828000

BS-DFT Optimised Coordinates

M06/def2-TZVPP level of theory

Energies are in Hartree (hf)

Complex **1′**

E = -3139.8400344Eh

42	0.001474000	-0.000631000	0.112902000
16	6.762198000	-0.006272000	0.278350000
16	-6.761388000	0.006259000	0.291675000
8	0.005243000	-0.001821000	1.755959000
7	4.309838000	1.102757000	-0.151115000
7	4.319729000	-1.090632000	-0.139724000
7	-4.319125000	1.090625000	-0.127444000
7	-4.309762000	-1.102782000	-0.141902000
6	5.141737000	0.009089000	-0.003151000
6	3.031174000	-0.703505000	-0.364358000
6	3.027270000	0.698945000	-0.368540000
6	-3.027322000	-0.699007000	-0.360156000
6	-3.030924000	0.703514000	-0.354038000
6	-5.141241000	-0.009099000	0.008462000
16	-1.652615000	1.681403000	-0.579322000
16	1.653255000	1.681880000	-0.587945000
16	-1.653844000	-1.681987000	-0.582898000
16	1.652671000	-1.681329000	-0.589026000
6	4.728192000	2.481086000	-0.057128000
1	5.775105000	2.497576000	0.234682000
1	4.605317000	2.979750000	-1.018168000
1	4.120765000	2.995605000	0.686636000
6	4.791277000	-2.450801000	-0.020682000
1	3.926644000	-3.108608000	0.020958000

1	5.415590000	-2.714311000	-0.873606000
1	5.385373000	-2.549868000	0.885793000
6	-4.728566000	-2.481089000	-0.049451000
1	-5.775587000	-2.497501000	0.241996000
1	-4.605545000	-2.978766000	-1.010977000
1	-4.121635000	-2.996639000	0.694000000
6	-4.790448000	2.450731000	-0.006466000
1	-3.925766000	3.108423000	0.035821000
1	-5.414954000	2.715427000	-0.858889000
1	-5.384330000	2.548622000	0.900275000

Complex **2′**

E = -7146.4168083Eh

42	-0.006333000	0.000422000	0.203513000
8	-0.022441000	0.001863000	1.846834000
7	-4.325222000	-1.103067000	-0.167174000
7	-4.339062000	1.083731000	-0.163112000
7	4.342057000	-1.084792000	-0.149529000
7	4.328819000	1.102116000	-0.156866000
6	-5.155908000	-0.013955000	-0.056379000
6	-3.041381000	0.699761000	-0.340127000
6	-3.035547000	-0.701002000	-0.341296000
6	3.037795000	0.700390000	-0.320272000
6	3.043253000	-0.700873000	-0.316948000
6	5.159963000	0.012835000	-0.050456000
16	1.655349000	-1.679926000	-0.478934000
16	-1.652284000	-1.683712000	-0.508329000
16	1.654409000	1.683717000	-0.480034000
16	-1.654149000	1.678467000	-0.512755000
6	-4.738583000	-2.485307000	-0.090365000
1	-5.784619000	-2.513318000	0.203853000
1	-4.614089000	-2.970176000	-1.058155000
1	-4.123534000	-3.003588000	0.644102000

6	-4.803855000	2.449808000	-0.068613000
1	-3.933772000	3.100946000	-0.038036000
1	-5.424963000	2.701314000	-0.927075000
1	-5.396262000	2.572250000	0.836036000
6	4.743776000	2.484271000	-0.085821000
1	5.792158000	2.512058000	0.199970000
1	4.611968000	2.967415000	-1.053489000
1	4.135288000	3.004465000	0.652705000
6	4.807665000	-2.450877000	-0.057260000
1	3.938012000	-3.102236000	-0.021025000
1	5.423451000	-2.702614000	-0.919486000
1	5.405801000	-2.572822000	0.843668000
34	-6.947812000	-0.002598000	0.177456000
34	6.953259000	0.001264000	0.171301000

13. References

[S1] Y. Wang, H. P. Hickox, Y. Xie, P. Wei, S. A. Blair, M. K. Johnson, III, H. F. Schaefer, G. H. Robinson, *J. Am. Chem. Soc*. 2017, **139**, 6859.

[S2] S. Das, A. Jain, S. Ahamed, B. Sahu, S. Suthar, B. Schwarz, C. L. Mascarenhas, S. Mondal, S. K. Kushvaha, S. Banerjee, H. W. Roesky and K. C. Mondal. *Angew. Chem. Int. Ed*. 2025, **64**, e202507231.

[S3] S. Stoll and A. Schweiger, EasySpin, *J. Magn. Reson.,* 2006, **178**, 42–55

[S4] P. Bertrand, *Electron Paramagnetic Resonance Spectroscopy: Fundamentals*, Springer; 2020th edition (4 February 2021); ISBN-10: 3030396657, ISBN-13: 978-3030396657.

[S5] R. Hille, C. Schulzke and M. L. Kirk, *Molybdenum and Tungsten Enzymes: Spectroscopic and Theoretical Investigations*; 2016th edition (10 October 2016); PDF ISBN-978-1-78262-884-2, EPUB ISBN-978-1-78262-885-9; *Chapter 3, Electron paramagnetic resonance studies of molybdenum enzymes*, S. Grimaldi, F. Biaso, B. Burlat and B. Guigliarelli.

[S6] I. K. Dhawan and J. H. Enemark, *Inorg. Chem*., 1996, **35**, 4873–4882.

[S7] (a) C. Balagopalakrishna, J. T. Kimbrough and T. D. Westmoreland, *Inorg. Chem.*, 1996, **35**, 7758. (b) M. A. Struwe, P. Kalimuthu, Z. Luo, Q. Zhong, D. Ellis, J. Yang, K. C. Khadanand, J. R. Harmer, M.

L. Kirk, A. G. McEwan, B. Clement, P. V. Bernhardt, B. Kobe and U. Kappler, *J. Biol. Chem*., 2021, **296**, 100672.

[S8] A. D. Becke, *Phys. Rev. A: At., Mol., Opt. Phys.* 1988, **38**, 3100.

[S9] Y. Zhao and D. Truhlar, *Theor. Chem. Acc.* 2008, **120**, 241.

[S10] S. Weigend and R. Ahlrichs, *Phys. Chem. Chem. Phys.* 2005, **7**, 3305.

[S11] A. D. Becke, *J. Chem. Phys.* 1993, **98**, 5652.

[S12] C. Lee, W. Yang and R. G. Parr. *Phys. Rev. B: Condens. Matter Mater. Phys.* 1988, **37**, 789.

[S13] A. D. Becke, *Phys. Rev. A*, 1988, **38**, 3098.

[S14] J. Tao, J. P. Perdew, V. N. Staroverov, and G. E. Scuseria, *Phys. Rev. Lett.* 2003, **91**, 146401.

[S15] Gaussian 16, Revision A.03, Frisch, M. J.; Trucks, G. W.; Schlegel, H. B.; Scuseria, G. E.; Robb, M. A.; Cheeseman, J. R.; Scalmani, G.; Barone, V.; Petersson, G. A.; Nakatsuji, H.; Li, X.; Caricato, M.; Marenich, A. V.; Bloino, J.; Janesko, B. G.; Gomperts, R.; Mennucci, B.; Hratchian, H. P.; Ortiz, J. V.; Izmaylov, A. F.; Sonnenberg, J. L.; Williams-Young, D.; Ding, F.; Lipparini, F.; Egidi, F.; Goings, J.; Peng, B.; Petrone, A.; Henderson, T.; Ranasinghe, D.; Zakrzewski, V. G.; Gao, J.; Rega, N.; Zheng, G.; Liang, W.; Hada, M.; Ehara, M.; Toyota, K.; Fukuda, R.; Hasegawa, J.; Ishida, M.; Nakajima, T.; Honda, Y.; Kitao, O.; Nakai, H.; Vreven, T.; Throssell, K.; Montgomery, J. A., Jr.; Peralta, J. E.; Ogliaro, F.; Bearpark, M. J.; Heyd, J. J.; Brothers, E. N.; Kudin, K. N.; Staroverov, V. N.; Keith, T. A.; Kobayashi, R.; Normand, J.; Raghavachari, K.; Rendell, A. P.; Burant, J. C.; Iyengar, S. S.; Tomasi, J.; Cossi, M.; Millam, J. M.; Klene, M.; Adamo, C.; Cammi, R.; Ochterski, J. W.; Martin, R. L.; Morokuma, K.; Farkas, O.; Foresman, J. B.; Fox, D. J. Gaussian, Inc., Wallingford CT, 2016.

[S16] E. D. Glendening, C. R. Landis and F. Weinhold, *J. Comput. Chem.* 2013, **34**, 1437.

[S17] A. E. Reed, L. A. Curtiss and F. Weinhold, *Chem. Rev.* 1988, **88**, 926.

[S18] F. Neese, *J. Phys. Chem. Solids*, **2004**, ***65***, 781–785.

[S19] M. Nakano, *Top. Curr. Chem.*, **2017**, ***375***, 47.

[S20] S. Ito, T. Minami and M. Nakano, *J. Phys. Chem. C*, **2012**, ***116*** **,**19729–19736.